Saturation of electrostatic instability in two-species plasma

N. J. B A L M F O R T H[1] and R. R. K E R S W E L L[2]

[1]Department of Applied Mathematics and Statistics, School of Engineering, University of California at Santa Cruz, CA 95064, USA

[2]Department of Mathematics, University of Bristol, Bristol BS8 1TW, UK

Abstract. We explore the level of saturation of instabilities in a two-species plasma using a combination of matched asymptotic expansion and numerical computation. The plasma is assumed to be spatially periodic, and the domain size is chosen to allow a single mode to become unstable when a bump is added to the tail of the distribution of the lighter species. We consider two versions of the problem, arising when the mass ratio of the two species is either very small, or of the order of unity. For small mass ratios, the initial saturation level of the mode amplitude, as measured by the electric field disturbance, follows the 'trapping scaling'. For mass ratios of order unity, nonlinear effects become important at the level predicted by Crawford and Jayaraman, but the instability does not saturate there and continues to grow. In both cases, the initial onset of nonlinearity does not reflect the longer-time evolution of the system. In fact, the system passes through multiple stages of evolution in which the electric field amplitude is not simply predicted; none of the previously published scalings are adequate. Eventually, for both cases, the distribution of the lighter ions becomes significantly rearranged, and much (though not all) of the destabilizing bump is flattened. A better predictor of the strength of the instability is given by the extent of these rearrangements.

---

1. Introduction

A classical problem in plasma theory is how electrostatic instabilities develop in the nonlinear regime. Some of the key previous results date back to Frieman et al. (1963), O'Neil et al. (1971), Onishchenko et al. (1971), and Simon and Rosenbluth (1976). All of these articles treat the single-species Vlasov equation, assuming that the lighter ions adjust in the instability, but the heavier ions are fixed in place. One of the striking features of the results is a disagreement regarding how the amplitude of saturation in the associated electric field disturbance, A_{sat}, scales with the distance to the stability boundary, as measured by a suitable control parameter, ϵ (proportional to the growth rate). Two characteristic scalings were hypothesized: 'trapping scaling', in which $A_{\mathrm{sat}} \sim \epsilon^2$ (O'Neil et al. 1971; Onishchenko et al. 1971), and Hopf scaling (e.g. Frieman et al. 1963; Simon and Rosenbluth 1976), $A_{\mathrm{sat}} \sim \epsilon^{1/2}$, which is the usual saturation level for strongly dissipative instabilities. The disparity arises because the system is not a dissipative one and the usual weakly nonlinear analysis is plagued by technical difficulties associated with singularities at the

'wave–particle resonance'. None of the original approaches convincingly dealt with these singularities, with the result that the effort to distinguish between them fell to numerical simulation and laboratory experiments. These suggested that trapping scaling dictates the saturation level (e.g. Denavit 1981).

Much more recently, two articles have convincingly demonstrated that the correct scaling for a single species is trapping (Crawford 1995; del Castillo-Negrete 1998). Crawford's approach follows the centre-manifold route and attempts to derive an amplitude equation for the unstable mode. However, the approach essentially begins with Hopf scaling and runs into technical complications associated with integrals that diverge at the wave–particle resonance as $\epsilon \to 0$. Rather than treating the singularities with some *ad hoc* rule, Crawford rescaled the mode amplitude with sufficient powers of ϵ in order to counter the divergent integrals. This procedure rescales the mode amplitude back to the trapping scaling and avoids a singularity, which formally establishes that trapping is the correct level of saturation. Unfortunately, Crawford's amplitude equation contains an infinite number of terms of comparable size and cannot be used to explore how the instability saturates.

Del Castillo-Negrete opts for a different approach based on the critical-layer theory of fluid mechanics. In fact, the saturation of instabilities in inviscid fluid shear flow is a close analogue of the plasma problem. The role of the wave–particle resonance is played by the 'critical level' – the surface along which the mean fluid flow equals the phase speed of a wave (and leads to Kelvin's 'disturbing singularity'). In fluid mechanics, it was recognized that the singularities at the critical level signified a breakdown of the asymptotic expansion procedure within a narrow region surrounding the critical level, the critical 'layer', and several articles (e.g. Churilov and Shukhman 1987) exploited matched asymptotic expansions to heal the singularity. The scaling required in the matched asymptotics is equivalent to trapping, and del Castillo-Negrete thereby derived the single-wave model systematically.

Most recently, Crawford and Jayaraman (1996, 1999) added a new facet to the problem. By repeating Crawford's analysis, they suggested that if the heavy-ion component of the plasma was allowed to be mobile, then trapping scaling would no longer be the correct predictor of saturation. Instead, they claim that a new scaling, $A_{\text{sat}} \sim \epsilon^{5/2}$, predicts the saturation level. Again, however, the analysis does not lead to a predictive model, only the amplitude scaling. Interestingly, there is a parallel result to this scaling in fluid mechanics found by Hickernell (1984). He observed that if the unstable mode was not smooth as it is limited to the stability boundary, which underlies the analysis leading to the single-wave model, but was singular instead, then $A_{\text{sat}} \sim \epsilon^{5/2}$. Subsequently, the 'singular' scaling was found in unstable compressible and stratified shear flows (Goldstein and Leib 1989; Churilov 1999). In fact, as we will see below, in the mobile ion problem, the neutral modes on the stability boundary are singular and Crawford and Jayaraman's scaling is exactly the plasma analogue of Hickernell's.

The aim of the current paper is to flesh out the nonlinear theory for the mobile-ion problem, using a combination of matched asymptotics and numerical computations. We show that the nonlinear dynamics of the two-species problem is much more complicated than the single-species case; the instability passes through various phases of evolution, each characterized by different scalings for the strength of the instability. As a result, none of the predicted amplitude scalings correctly predicts the saturation level. Worse still, we find that the electric field disturbance is a

poor measure of the overall strength of the instability. We offer a more useful characterization in our conclusion.

In the following, we first formulate the mathematical problem (Sec. 2) and then consider two characteristic limits that demand different angles of attack. The first limit (Sec. 3) is when the mass ratio is so small that it is comparable to, or smaller than, ϵ. In this limit, we recover the trapping scaling for the saturation level of instabilities, but there are some twists in the tale. The second limit (Sec. 4) is when the mass ratio is not so disparate, ϵ is the smallest parameter of the problem, and we encounter the singular scaling. Unfortunately, in neither limit does the weakly nonlinear theory capture the long-time dynamics of the instability. We turn to numerical computations to explore the late-time evolution (Sec. 5).

2. The problem

2.1. Formulation

The governing, dimensionless equations for a two-species, one-dimensional plasma are:

$$f_t^{(j)} + v f_x^{(j)} + \kappa^{(j)} \varphi_x f_v^{(j)} = 0, \qquad j = 1, 2, \tag{2.1}$$

with

$$\varphi_{xx} = \int_{-\infty}^{\infty} [f^{(2)}(x, v, t) - f^{(1)}(x, v, t)] \, dv + \Psi_{xx}, \tag{2.2}$$

where $f^{(j)}(x, v, t)$ denote the distribution functions of the two species, $\varphi(x, t)$ is the potential of the total electric field and $\Psi(x, t)$ denotes a small external field perturbation that we will exploit later to kick the system off an equilibrium solution and into action. The first species we specify to be negative ions (we informally refer to them as electrons); the particle mass and charge of this species are used to non-dimensionalize the equations, leading to $\kappa^{(1)} = -1$. The other species is positively charged and $\kappa^{(2)} \equiv \kappa = |(e_2 m_1)/(e_1 m_2)|$, a positive parameter which we take to be less than unity.

We assume periodic boundary conditions in x (and denote the domain size by L); in v, we insist that $f^{(j)}$ should remain bounded as $v \to \pm\infty$. As indicated above, the initial condition will be an equilibrium solution that is subsequently disturbed by the external field $\Psi(x, t)$. Equally well, however, we could take $\Psi = 0$ and consider an initial state containing the equilibrium plus a perturbation with the form of a low-amplitude instability wave. Either way, the nonlinear theory is little different since the excited instability grows exponentially to dominate the dynamics.

The equilibria of the system that we consider are the spatially homogeneous states, $f^{(j)} = F^{(j)}(v)$. By way of an example, we take the family given by

$$F^{(1)}(v) = e^{-v^2} + a e^{\lambda(v-v_0)^2} \qquad \text{and} \qquad F^{(2)}(v) = e^{-bv^2}, \tag{2.3}$$

where a, λ, b and v_0 are parameters, although the total charge neutrality of the plasma requires that $b = (1 + a/\sqrt{\lambda})^{-2}$. An example is shown in Fig. 1. This parametrized family consists of an electron distribution with a classical 'bump-on-tail', together with a simpler ion distribution. Practically, we fix the parameters λ and v_0 (we take $\lambda = 4$ and $v_0 = 2$). The parameter a then controls the size of the bump, and we anticipate instability beyond some critical threshold in a.

In our asymptotic analyses, an alternative formulation of the equations makes

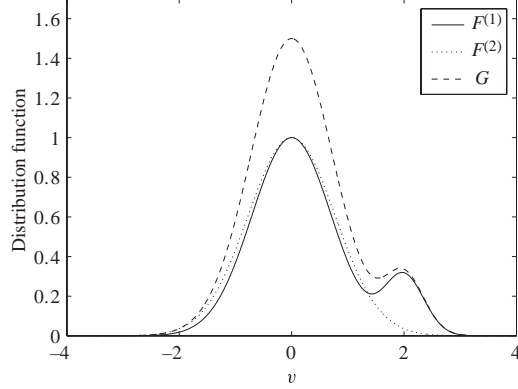$$a = 0.3, \kappa = 0.5, \lambda = 4, v_0 = 2$$

Figure 1. An example equilibrium profile with $a = 0.3$, $\kappa = 0.5$, $\lambda = 4$ and $v_0 = 2$;
b is determined by the condition of no net charge.

the formal derivations a little clearer: let $g(x, v, t) = f^{(2)} - f^{(1)} - F^{(2)} + F^{(1)}$ and
$h(x, v, t) = f^{(2)} + f^{(1)} - F^{(2)} - F^{(1)}$. Then,

$$g_t + v g_x + \varphi_x G' + \left(\frac{\kappa - 1}{2} g_v + \frac{\kappa + 1}{2} h_v \right) \varphi_x = 0, \qquad (2.4a)$$

$$h_t + v h_x + \varphi_x H' + \left(\frac{\kappa + 1}{2} g_v + \frac{\kappa - 1}{2} h_v \right) \varphi_x = 0 \qquad (2.4b)$$

and

$$\varphi_{xx}(x, t) = \int_{-\infty}^{\infty} g(x, v, t) \, dv + \Psi_{xx}(x, t), \qquad (2.5)$$

where $G = F^{(1)} + \kappa F^{(2)}$ and $H = \kappa F^{(2)} - F^{(1)}$.

2.2. Linear theory

We set $[g, h] = [\hat{g}(v), \hat{h}(v)] e^{ik(x - ct)} + \text{c.c.}$ and $\varphi = \hat{\varphi} e^{ik(x - ct)} + \text{c.c.}$, and then linearize
the equations in the perturbation amplitudes. With our periodic-in-x boundary
conditions, $k = 2n\pi/L$ for $n = 0, 1, 2, \ldots$. The eigenvalues, c, are determined by the
relations,

$$\hat{g} = -\frac{\varphi G'}{v - c}, \qquad \varphi = -\frac{1}{k^2} \int_{-\infty}^{\infty} \hat{g} \, dv. \qquad (2.6)$$

It is now straightforward to find the dispersion relation,

$$1 - \frac{1}{k^2} \int_{-\infty}^{\infty} \frac{G'(v) \, dv}{v - c} = 0. \qquad (2.7)$$

This relation is identical in form to that for the single-species Vlasov problem,
and we mention a few of its properties that bear upon the current problem: the
dispersion relation contains a singular integral with a branch cut along the real
axis of the complex c plane; the cut locates the continuous spectrum of the lin-
ear eigenvalue problem. Complex conjugate solutions for c correspond to discrete,
growing/decaying mode pairs; the mode with $c_i > 0$ is unstable. There must be at
least two peaks in the distribution $G(v)$ in order for such modes to exist (and there-
fore for the equilibrium to be unstable). Two neutral stability conditions follow on

using the Plemelj relation with $c \to c_*$, c_* real:

$$G'(c_*) = 0 \qquad \text{and} \qquad k^2 = \int_{-\infty}^{\infty} \frac{G'(v)\, dv}{v - c_*}. \qquad (2.8)$$

These define the neutral modes that connect the complex conjugate pairs to the continuous spectrum as one proceeds along a parametrized sequence of equilibrium profiles; that is, (2.8) defines the embedded neutral modes on the stability boundary. Evidently, these modes have wave speeds defined by the extremal points of $G(v)$, and arise for certain values of the control parameter, a, such that the wavenumber given by the integral in (2.8) is consistent with that demanded by the domain size. For our sample equilibrium profiles, we parametrize the stability boundary by the curves $a = a_0(k)$. Such curves are illustrated in Fig. 2.

Nevertheless, the construction of the stability boundary misses a key feature of the two-species problem: in deriving (2.7), we take no account of the field, h, since this does not enter into the integral for the perturbation to the electric potential. However, this field is characterized by the eigenfunction,

$$\hat{h} = -\frac{\varphi H'}{v - c}. \qquad (2.9)$$

Furthermore, even though $G'(c_*)$ must vanish on the stability boundary, as in (2.8), there is no corresponding constraint on $H'(c_*)$, which, in general, will not vanish. Thus, the perturbation amplitude $\hat{h}(v)$ is singular at the critical point $v = c_*$ (the wave–particle resonance). Hence, despite the existence of a well-defined stability boundary with its associated wave speed $c_*(a)$, the corresponding normal modes are not smooth eigensolutions. This has crucial ramifications upon both the linear and nonlinear development of weakly unstable modes, and is the source of the change of scaling observed by Crawford and Jayaraman. In the weakly nonlinear theories outlined below, the singularity in the normal-mode solution is healed by adding unsteadiness and nonlinearity.

3. Nonlinear theory for disparate masses ($\kappa \ll 1$)

We first analyse the weakly nonlinear dynamics for $\kappa \ll 1$. We specify $k = 2\pi/L$, thence a point on the stability boundary $a = a_0(k)$, and demand that there are no other unstable or neutral modes with different wavenumbers. This distinguishes a special neutral mode with which we may open an asymptotic expansion. The expansion proceeds by displacing the system a small distance from the stability boundary, as measured by our control parameter, $a = a_0 + \epsilon$. We then set $\kappa = \epsilon \kappa_1$, to ensure disparate ion masses. Provided we are not at the minimum of the stability boundary, the distinguished mode has a pattern speed that lines up with either the peak or the trough of the destabilizing bump; at the minimum, the mode's pattern speed lines up with the inflection point of the unperturbed equilibrium profile (see Fig. 2). In both cases, the development of the equations is a simple generalization of the theory for a single species which gives the single-wave model.

3.1. Trapping scalings and outer expansion

For ease of notation, in what follows, we adjust the origin of v such that the neutral mode has zero wave speed (that is, $c_*(a_0) = 0$) and pick $L = 2\pi$ (so $k = 1$), but neither
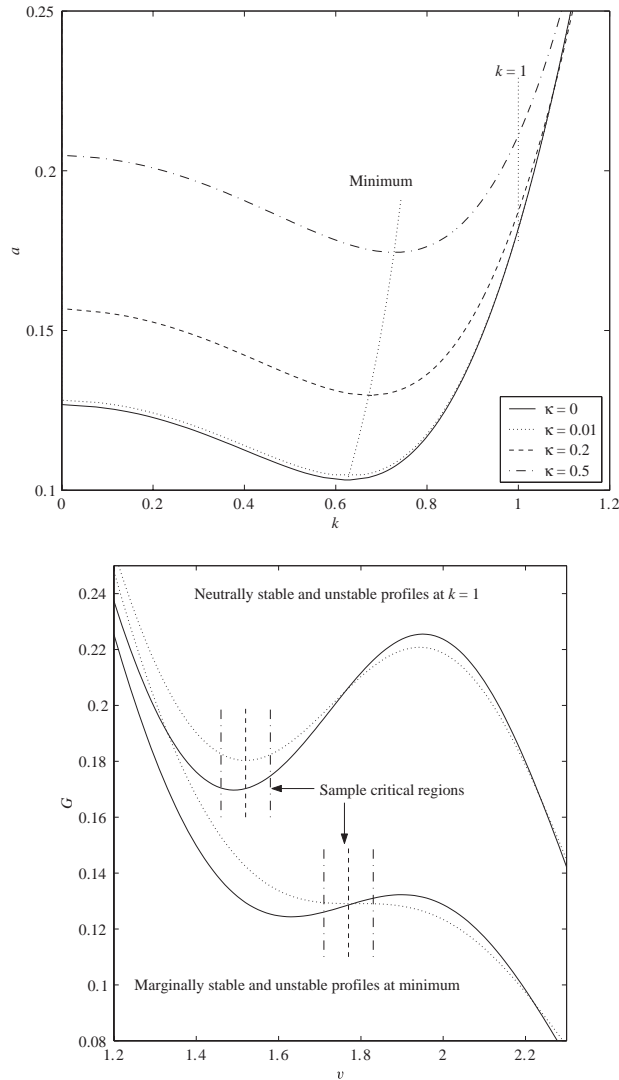
Figure 2. Sample stability boundaries on the (a, k)-plane for the equilibrium profiles (2.3) with $\lambda = 4$ and $v_0 = 2$. The four curves show four values of κ. The locus of the minimum of the stability boundary as κ varies is also indicated, as is the line $k = 1$ along which we perform most of our computations. The lower panel shows a magnification of the velocity range surrounding the destabilizing bump in the distribution function $G(v)$. Two pairs of equilibrium profiles are shown. The dotted curves represent profiles on the stability boundary at the minimum (where all wavenumbers are stable) and for $k = 1$. The solid curves show neighbouring unstable equilibria. Also illustrated are the corresponding 'critical regions' – the velocities surrounding the pattern speed of the neutral mode on the stability boundary (shown by dashed lines) over which the distribution function is wound up as the mode grows when it is made unstable. These regions are always much narrower than the velocity spread of the bump.

choice is essential.† We then introduce the (trapping) scalings and sequences,

$$\partial_t \rightarrow \epsilon \partial_T, \qquad a = a_0 + \epsilon, \qquad G(v) = G_0(v) + \epsilon G_1(v), \qquad H(v) = -G_0(v) + \epsilon H_1(v), \tag{3.1}$$

and

$$g(x, v, t) = \epsilon^2 g_2(x, v, T) + \epsilon^3 g_3(x, v, T) + \cdots, \tag{3.2a}$$

$$h(x, v, t) = \epsilon^2 h_2(x, v, T) + \epsilon^3 h_3(x, v, T) + \cdots, \tag{3.2b}$$

$$\varphi(x, t) = \epsilon^2 \varphi_2(x, T) + \epsilon^3 \varphi_3(x, T) + \cdots, \tag{3.3a}$$

$$\Psi(x, t) = \epsilon^3 \Psi_3(x, T), \tag{3.3b}$$

where $G_0(v) \equiv -H_0(v)$ is the neutrally stable equilibrium profile determined by $a = a_0$ and $\kappa = 0$, and G_1 and H_1 arise from the correction to a and κ_1. In the initial state, $g(x, v, 0) = h(x, v, 0) = 0$, and the external perturbation $\epsilon^3 \Psi_3(x, T)$ will turn on the unstable mode.

We introduce the scalings and sequences into the governing equations and gather terms of like order in ϵ. At leading order (ϵ^2),

$$g_2 = -\frac{G_0'}{v} \varphi_2 = -h_2 \qquad \text{and} \qquad \varphi_{2xx} = \int_{-\infty}^{\infty} g_2 \, dv, \tag{3.4}$$

with solution,

$$\varphi_2 = A(T) e^{ix} + \text{c.c.} \qquad \text{and} \qquad g_2 = -\frac{G_0'}{v} A(T) e^{ix} + \text{c.c.} = -h_2, \tag{3.5}$$

given that the neutral stability point demands that

$$1 = \int_{-\infty}^{\infty} \frac{G_0'(v) \, dv}{v}. \tag{3.6}$$

As yet, the amplitude, $A(T)$, is undetermined; our goal is an evolution equation for $A(T)$ (with initial condition $A(0) = 0$).

At the following order (ϵ^3),

$$g_3 = -\frac{G_0'}{v} \varphi_3 - \frac{G_1'}{v} (A e^{ix} + \text{c.c.}) - \frac{G_0'}{v^2} (i A_T e^{ix} + \text{c.c.}), \tag{3.7}$$

with a similar result for h_3. At this stage, we are not able to integrate g_3 over v to formulate φ_3 because that function is singular at the critical point, $v = 0$ – in general, $G_0''(0) \neq 0$ and $G_1'(0) \neq 0$. The way around the problem is not to introduce an *ad hoc* mathematical rule for by-passing the singular point, but to realize that the asymptotic scheme has formally broken down in its vicinity. In particular, because $g_2 \sim O(1)$ and $g_3 \sim v^{-1}$ near $v = 0$, we see that the asymptotic sequence $\epsilon^2 g_2 + \epsilon^3 g_3$ becomes disordered when $v = O(\epsilon)$. Over this region we cannot use the regular solution derived above. Instead, we must rescale and look for an alternative solution inside this 'inner' region; illustrations of the 'critical region' are shown in Fig. 2. This region is the site of the capture of resonant electrons by the potential of the growing wave, in the classical vision of electrostatic instability, and is analogous to the critical layer of fluid mechanics. The complete solution is

† By defining the new variables, $\tilde{t} = kt$, $\tilde{x} = kx$, $\tilde{v} = v - v_*$ and $\tilde{f}^{(j)} = f^{(j)}/k^2$, where v_* denotes the critical level of the neutral mode on the stability boundary, we may recast the equations for general k into the form of the system with $k = 1$ and $c_*(a_0) = 0$.

found by matching the two different expansions over an intermediate matching region, as in any matched asymptotic expansion.

3.2. *The critical region*

We rescale to resolve the critical region – the order ϵ region around $v = 0$:

$$v \to \epsilon Y, \qquad g(x, v, t) \to \epsilon^2 Z(x, Y, T), \qquad h(x, v, t) \to \epsilon^2 W(x, Y, T), \qquad (3.8)$$

$$G_0'(v) \to \epsilon Y G_{0*}'' + \cdots, \qquad G_1'(v) \to G_{1*}' + \cdots, \qquad H_1'(v) \to H_{1*}' + \cdots, \qquad (3.9)$$

where the $*$ subscript denotes the value at $v = 0$. The governing equations become, to leading order,

$$\left. \begin{aligned} Z_T + Y Z_x - \tfrac{1}{2} \varphi_{2x}(Z - W)_Y &= -Y G_{0*}'' \varphi_{2x} - G_{1*}' \varphi_{2x}, \\ W_T + Y W_x + \tfrac{1}{2} \varphi_{2x}(Z - W)_Y &= Y G_{0*}'' \varphi_{2x} - H_{1*}' \varphi_{2x}. \end{aligned} \right\} \qquad (3.10)$$

Let $2z = Z - W$ and $2w = Z + W$. Then,

$$\left. \begin{aligned} z_T + Y z_x - \varphi_{2x} z_Y &= -Y G_{0*}'' \varphi_{2x} - \tfrac{1}{2}(G_{1*}' - H_{1*}') \varphi_{2x}, \\ w_T + Y w_x &= -\tfrac{1}{2}(G_{1*}' + H_{1*}') \varphi_{2x} = -\kappa_1 F_{v*}^{(2)} \varphi_{2x}. \end{aligned} \right\} \qquad (3.11)$$

The first of these is a nonlinear partial differential equation that cannot be solved in closed form, but must be solved numerically. The second relation is linear and, given the form of φ_2, has the solution,

$$w = -i\kappa_1 F_{v*}^{(2)} \int_0^T \left[A(s) e^{ix + iY(s-T)} + \text{c.c.} \right] ds. \qquad (3.12)$$

Below we require an integral of the solution over the critical region:

$$\frac{1}{2\pi} \int_0^{2\pi} \int_{-\infty}^{\infty} w(x, Y, T) e^{-ix} \, dY \, dx \equiv -i\pi \kappa_1 F_{v*}^{(2)} A. \qquad (3.13)$$

3.3. *The match*

The final piece of the puzzle is to match the two parts of the solution over a matching region, and then compute the integral determining φ_3. The large Y behaviour of $z(x, Y, T)$ and $w(x, Y, T)$ is given by

$$z \sim -G_{0*}'' \varphi_2 - \frac{1}{2Y}(G_{1*}' - H_{1*}') \varphi_2 + \frac{1}{Y} G_{0*}'' \varphi_{2xT} \qquad \text{and} \qquad w \sim -\frac{1}{Y} \kappa_1 F_{v*}^{(2)} \varphi_2, \quad (3.14)$$

and one can immediately match the inner and outer distribution functions. We next define a solution for g to order ϵ^3 that is uniformly valid over all v by using the usual prescription, inner + outer − match. The integral of this construct gives

$$\epsilon^2 \int_{-\infty}^{\infty} g_2(x, v, T) \, dv + \epsilon^3 \mathscr{P} \int_{-\infty}^{\infty} g_3(x, v, T) \, dv + \epsilon^3 \mathscr{P} \int_{-\infty}^{\infty} [Z(x, v, T) - g_{2*}] \, dY + O(\epsilon^4), \qquad (3.15)$$

where $\mathscr{P}$ indicates the principal value of the v-integral at $v = 0$, or the Y-integral

at $\pm\infty$ (as indicated by (3.14), $Z - g_{2*} \equiv z + w + G''_{0*}\varphi_2$ decays like Y^{-1} for large $|Y|$). Thence,

$$\varphi_{3xx} = \mathscr{P} \int_{-\infty}^{\infty} g_3(x, v, T)\, dv + \mathscr{P} \int_{-\infty}^{\infty} [Z(x, Y, T) - g_{2*}]\, dY + \Psi_{3xx}. \qquad (3.16)$$

Finally, we let $z = \zeta(x, Y, T) - g_{2*}$ (implying $Z - g_{2*} = \zeta + w$), and isolate the e^{ix} component of (3.16):

$$iI_0 A_T + I_1 A + \hat{\Psi}_3(T) = \frac{1}{2\pi}\mathscr{P} \int_0^{2\pi}\int_{-\infty}^{\infty} e^{-ix}(\zeta + w)\, dY\, dx \equiv \langle e^{-ix}(\zeta + w)\rangle, \qquad (3.17)$$

where

$$I_0 = \mathscr{P} \int_{-\infty}^{\infty} \frac{G'_0}{v^2}\, dv, \quad I_1 = \mathscr{P} \int_{-\infty}^{\infty} \frac{G'_1}{v}\, dv \qquad (3.18)$$

and $\hat{\Psi}_3(T)$ is the relevant component of the forcing.

3.4. The modified single-wave model

We now summarize the results by quoting the complete set of equations after they have been transformed into a canonical form. We use the scalings

$$T = \tau T', \quad A = -\frac{1}{\tau^2}e^{iI_1 T/I_0}A', \quad \zeta = -\frac{|I_0|}{\tau^2}\zeta', \quad Y = \frac{1}{\tau}Y' - \frac{I_1}{I_0}, \quad x = x' - \frac{I_1}{I_0}\tau T', \qquad (3.19)$$

to find, after dropping the prime decoration,

$$\zeta_T + Y\zeta_x + \varphi_x\zeta_Y = -\beta\varphi_T - \gamma\varphi_x, \qquad (3.20)$$

$$\varphi = Ae^{ix} + \text{c.c.} \qquad \text{and} \qquad A_T = i\langle e^{-ix}\zeta\rangle - \mu A + \chi(T), \qquad (3.21)$$

where

$$\beta = \frac{G''_{0*}}{|I_0|}, \qquad \gamma = \frac{\tau}{|I_0|}\left(\frac{G'_{1*} - H'_{1*}}{2} + \frac{I_1}{I_0}G''_{0*}\right) \qquad \text{and} \qquad \mu = \frac{\pi\kappa_1\tau F'_{2*}}{I_0}, \qquad (3.22)$$

and we have used the fact that $I_0 < 0$ for our model equilibria; $\chi(T)$ is a suitably scaled forcing function. At this juncture, τ is still arbitrary; a convenient choice is to fix this constant such that $\gamma = \pm 1$. Also, the transformation, $\zeta \to -\zeta$, $Y \to -Y$, $A \to A^*$ and $x \to -x$, changes β into $-\beta$ but otherwise leaves the equations unchanged. Thence, we may consider β as purely positive.

We impose the boundary and initial conditions: $\zeta \sim O(Y^{-1})$ as $|Y| \to \infty$, $\zeta(x, Y, 0) = 0$ and $A(0) = 0$. The first of these repeats the need to interpret the critical region integral $\langle e^{-ix}\zeta\rangle$ in terms of a principal value at its limits in Y. Below, we solve the equations numerically, using a variant of the operator-splitting scheme proposed by Cheng and Knorr (1976; see Balmforth et al. 2000). We choose $\chi(T) = 0.1iT\exp(-50T^2)$, which corresponds to a certain potential function Ψ_3; the particular form of χ is computationally convenient, but not significant (it also differs from the forcing function used in the numerical computations of Sec. 5).

Except for the term involving μ, this system is identical to the model one derives for a single species, and is the canonical form of the single-wave model. Crucially important in the model are the two terms, $\gamma\varphi_x$ and $\beta\varphi_T$, which arise from gradients of the background equilibrium profiles. The first of these terms is exclusively responsible for instability in our canonical problem (see below). The formulation

is therefore different to the approach taken by del Castillo-Negrete (1998) who adopts $\beta = \gamma = 0$. Instead, del Castillo-Negrete follows the original development of the phenomenological single-wave model (O'Neil et al. 1971; Onishchenko et al. 1971) wherein instability is introduced via an arbitrary initial condition $\zeta(x, Y, 0)$. Here, we consider only the canonical problem.

The positive-ion effect, as gauged by μ, depends crucially on the sign of $F_{v*}^{(2)}/I_0$. The positive ions are stabilizing when $\mu > 0$, which is the case for our family of model equilibria. The stabilization originates from Landau damping in the positive-ion distribution. The destabilizing case, $\mu < 0$, requires a gradient reversal such as would be given by a bump on the tail of the positive-ion distribution (cf. Berk et al. 1999).

The model has an infinite number of conservation laws that it inherits from the original equations: let $q = \zeta + \beta(\varphi - Y^2/2) + \gamma Y$ denote the total distribution function within the critical region (satisfying $q_T + Y q_x + \varphi_x q_Y = 0$). Then, $\langle F(q) \rangle = \text{constant}$, for any function $F(q)$ consistent with a convergent integral, which expresses Casimir invariants. In addition, there are the global momentum and energy relations,

$$(\langle Y\zeta \rangle + |A|^2)_T = -2\mu |A|^2 \qquad \text{and} \qquad \left\langle \frac{1}{2} Y^2 \left(\zeta - \frac{\beta \varphi^2}{Y^2} \right) - \varphi \zeta \right\rangle_T = 2\mu \, \text{Im}(A^* A_T),$$

$$(3.23)$$

which apply once the forcing function χ has turned off. The global momentum condition proves useful below; Landau damping by positive ions enters explicitly as a sink of momentum in this formula.

3.5. Single-wave dynamics

3.5.1. Linear dynamics. We pause momentarily to give a quick summary of the linear theory. By dropping the nonlinear term, we find

$$\zeta = -\int_0^T e^{ix - iY(T-s)} \left(\beta \frac{dA}{ds} + i\gamma A \right) ds + \text{c.c.}, \qquad \langle e^{-ix}\zeta \rangle = -\pi(\beta A_T + i\gamma A),$$

$$(3.24)$$

from which it follows that

$$A_T - \frac{\pi\gamma - \mu}{1 + i\pi\beta} A = \frac{\chi(T)}{1 + i\pi\beta}.$$

$$(3.25)$$

Once the forcing subsides, $\chi \to 0$ and an exponential solution emerges:

$$A \sim \exp \left[\frac{(\pi\gamma - \mu)}{1 + \pi^2\beta^2}(1 - i\pi\beta)T \right].$$

$$(3.26)$$

The system is therefore unstable when $\pi\gamma > \mu$. If $\mu > \pi\gamma$, A decays exponentially through Landau damping.

3.5.2. Near marginal stability. We now focus on cases with $\mu \geqslant 0$ and $\gamma = 1$. First, we take $\beta = 0$, which corresponds to $G_{0*}'' = 0$ and requires that we perturb about the state at the minimum of the stability boundary – the marginally stable profile for all wavenumbers (see Fig. 2). The time series of $A(T)$ for several numerical computations with different μ are shown in Fig. 3. The initial phase of the instability is well predicted by the exponential growth of linear theory. This growth does not continue indefinitely, and eventually the system passes into a second phase of evolution in which the parameter μ plays a key role. For $\mu = 0$, the mode amplitude remains close to the initial saturation level, and persistent, irregular 'trapping
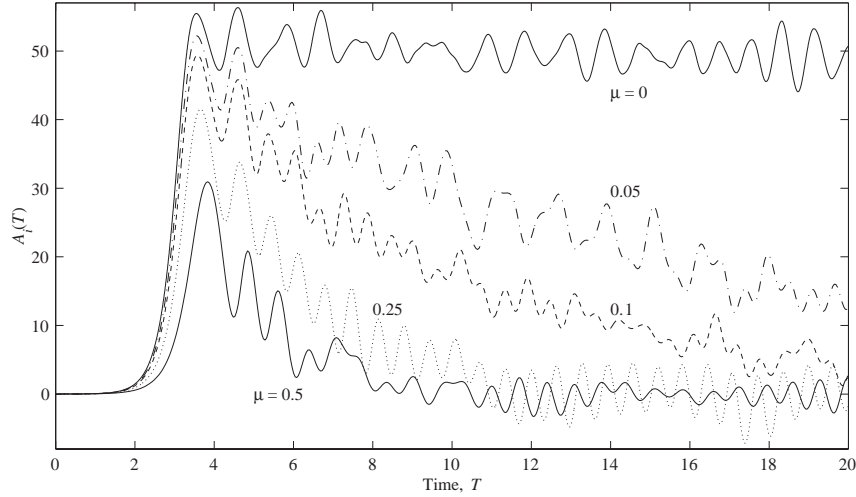
Figure 3. Time series of the mode amplitude for $\beta = 0$, $\gamma = 1$ and five values of μ. In this instance, the solution has the reflection symmetry, $\zeta(x, Y, T) = -\zeta(\pi - x, -Y, T)$ (which is exploited to double the resolution of the numerical computation) and $A(T)$ is purely imaginary. The figure shows $A_i(T)$.

oscillations' occur about some mean level. On the other hand, if $\mu \neq 0$, the mode amplitude declines beyond the initial maximum, with a decay that is roughly given by $\exp(-\mu T)$ (see Fig. 4), together with superposed trapping oscillations.

For the profile with $G''_{0*} = 0$, when we add the equilibrium correction, $G_1(v)$, to create the bump, the critical region sits at the centre of the unstable, positive gradient of the distribution function (Fig. 2). The destabilizing gradient is locally linear and competes with the damping provided by the positive ions. However, as the instability grows, it winds up the equilibrium profile of the electron distribution into a pattern of vortex-like structures (the analogue of Kelvin cat's eyes, or BGK modes – Bernstein, Greene and Kruskal 1958); see Fig. 4. This action removes the destabilizing gradients with the result that the mode amplitude begins to saturate. However, the destruction of the destabilizing gradients is permanent (there is no mechanism to restore the gradients once they are removed), but the damping of the positive ions continues all the while. As a result, beyond saturation, the damping takes greater effect and exacts its toll on the mode; $|A(T)|$ thereby declines, as seen in Fig. 3.

By this stage of the evolution, the shearing action of the basic electron velocity spread in tandem with the winding of the cat's eye generates fine scales in the distribution function. Any spatial averaging (including finite resolution and dissipation in the computation) removes much of this structure and in a coarse-grained sense the distribution function becomes flat. This smoothing action is illustrated by the x-average of $q = Y + \zeta(x, Y, T)$, which is also shown in Fig. 4.

Despite the positive-ion damping, the mode amplitude does not decay completely. Persistent, residual, trapping-like oscillations occur in $A(T)$, which can be traced to the emergence of coherent secondary cat's eye structures at the boundaries of the well-mixed central region (see Fig. 4). The structures are counter-propagating BGK waves and appear to emerge from a secondary instability of the distribution function after it has been restructured by the unstable mode.
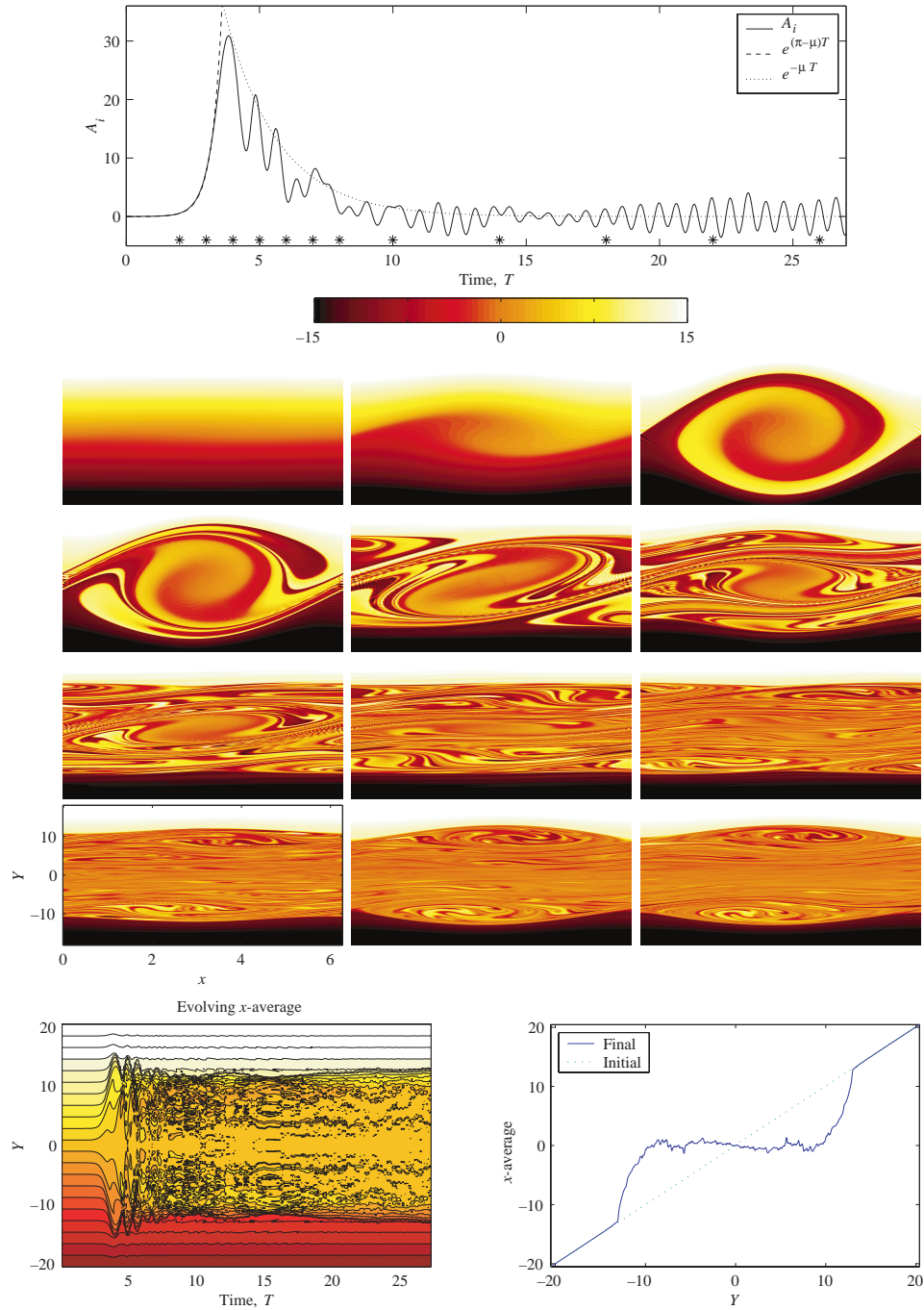
Figure 4. The top panel shows the evolution of the mode amplitude for $\beta = 0$ and $\mu = 0.5$. The linear growth, $\exp(\pi - \mu)T$, and the decay trend, $\exp(-\mu T)$, are also shown. The following panels show snapshots of the total distribution function inside the critical region, $q(x, Y, T) \equiv Y + \zeta(x, Y, T)$, plotted as a density on the (x, Y)-plane with the greyscale indicated. The times of the snapshots are $2, 3, \ldots, 8, 10, 14, 18, 22$ and 26 (and are indicated by stars in the top panel). The final plots show the evolution of the x-average of q (as contours on the (T, Y)-plane) and its initial and final profiles.
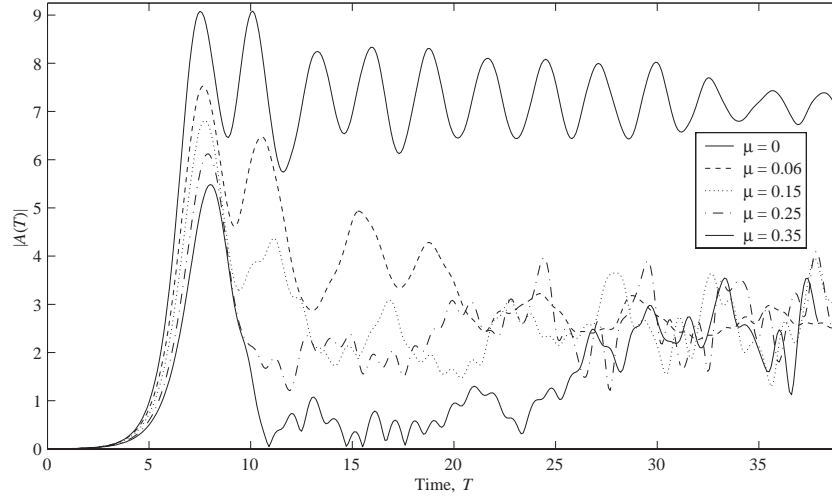
Figure 5. Time series of the mode amplitude for $\beta = 0.4$, $\gamma = 1$ and five different values of μ.

3.5.3. Further from marginality. When $\beta \neq 0$, the distinguished neutral mode on the stability boundary is centred either at the peak or the trough of the destabilizing bump; for $k = 1$, the critical region surrounds the trough. Although the equilibrium electron distribution is now locally parabolic within the critical region, the pattern of evolution is similar to the case with $\beta = 0$: the mode amplitude grows to saturation, and then declines due to the effect of the positive ions. Unlike $\beta = 0$, however, $A(T)$ recovers and then oscillates about a finite value (see Figs 5 and 6). Again the decline of the mode amplitude depends on μ (the decay is roughly $\exp(-\mu T)$), but the level to which the mode amplitude recovers appears to be independent of this parameter.

Because the mode amplitude levels off for finite β, the main cat's eye shrinks a little, but survives. At the same time, the cat's eye also begins to drift in Y, leaving a mixed region in its wake. The drift permits the mode to access fresh unstable gradients, which revives the instability and allows the cat's eye to survive the positive-ion damping. A complementary interpretation is provided by the global momentum constraint: if $|A|$ becomes roughly constant, $\langle Y\zeta \rangle \sim -2\mu|A|^2 T$. Moreover, because q is simply rearranged by the dynamics, the resonant contribution, $\langle Y\zeta \rangle$, can only decrease indefinitely if the region over which ζ is nonnegligible and negative spreads to larger Y with time. Thus, in order to sustain a finite-mode amplitude indefinitely, the cat's eye must continually drift; the computational solutions show drifts over relatively long times, and we conjecture that such a secular evolution is the fate of the system. Drifting coherent structures in two-species plasma simulations have been observed previously by Berman et al. (1985, 1986) and Berk et al. (1999).

The overall dynamics of the unstable mode is therefore largely a transient one: the mode grows, saturates, and then declines (there are some similarities with results presented by Berk et al. 1996, for a Vlasov equation with a simple linear damping term). Ultimately, the decline halts as cat's eye structures drift out of the critical region and into the unstable gradients beyond. The mode amplitude can be maintained indefinitely in this fashion because the quadratic background profile of the single-wave model contains a semi-infinite region with positive gradients. However, this is not a property of the underlying bump-on-tail distribution, for which
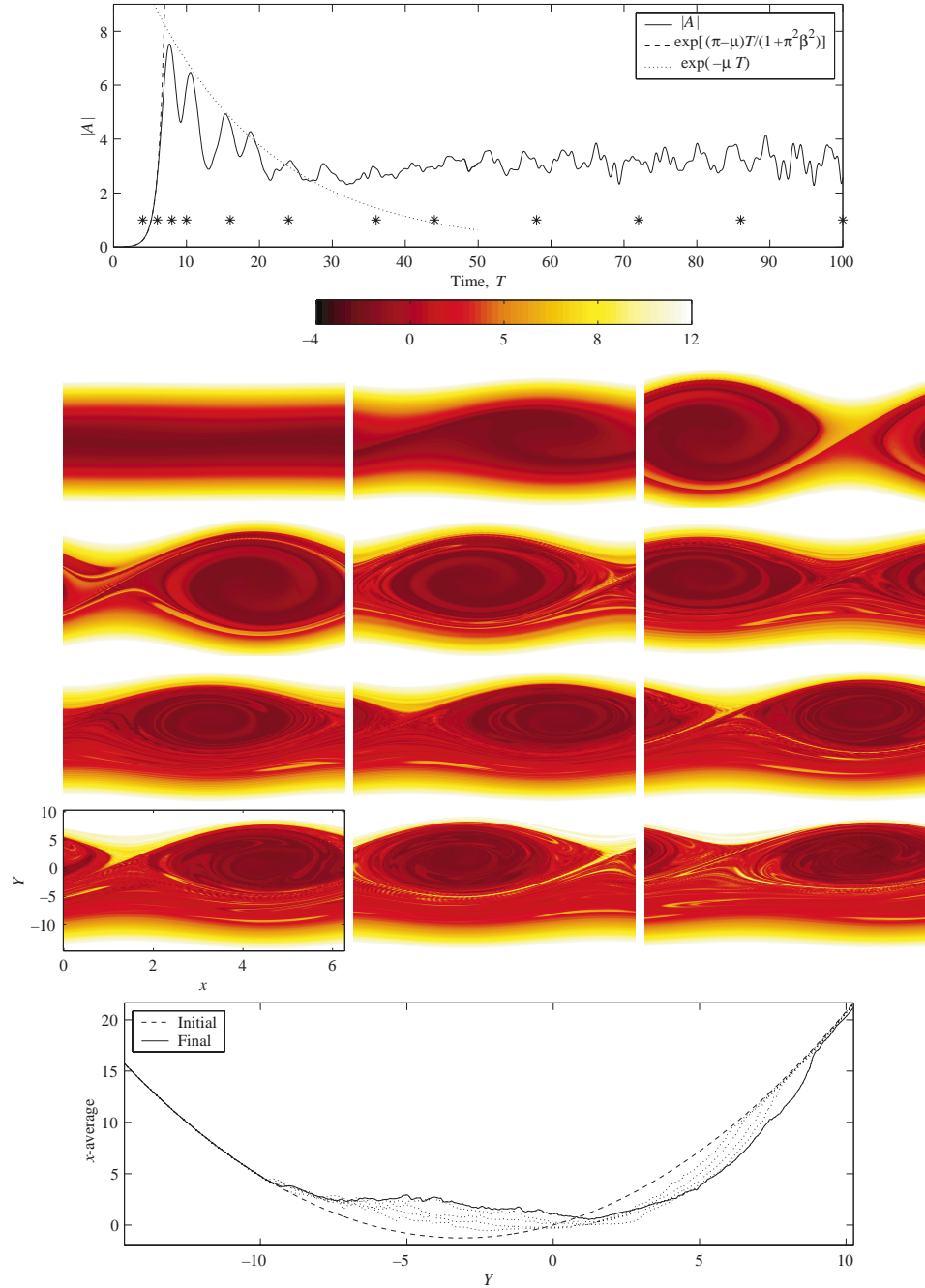
Figure 6. A computation with the modified single-wave model with $\beta = 0.4$ and $\mu = 0.06$. The top picture shows the evolving mode amplitude, together with the trends of linear growth, $\exp[(\pi - \mu)T/(1 + \pi^2\beta^2)]$, and positive-ion damping, $\exp(-\mu T)$. The following panels display snapshots of the total distribution function inside the critical region, $q \equiv \beta\varphi - \beta Y^2/2 + Y + \zeta(x, Y, T)$. The times of the snapshots are 4, 6, 8, 10, 16, 24, 36, 44, 58, 72, 86 and 100 (and are shown by stars in the top panel). The initial and final x-averages of q are shown in the final plot, together with the intermediate averages every 20 time units.

the unstable equilibrium gradients have a finite velocity range. Hence, in reality the drift of the cat's eye must eventually run out of steam and the system pass out of the trapping regime. We comment further on this passage later when we solve the two-species equations numerically.

4. Nonlinear theory in the 'generic' case, $\kappa \sim O(1)$

We now repeat the nonlinear theory for the case where $\kappa \sim O(1)$. In this case, the nonlinear dynamics of the positive ions enters into the problem and we no longer find the single-wave model, but another whose scalings were predicted by Crawford and Jayaraman (1996, 1999) and Hickernell (1984).

4.1. Regular expansion

The scalings and sequences are now

$$\partial_t \to \epsilon\partial_T, \qquad a = a_0 + \epsilon, \qquad G(v) = G_0(v) + \epsilon G_1(v), \qquad H(v) = H_0(v) + \epsilon H_1(v),$$
(4.1)

and

$$g = \epsilon^{5/2}g_{5/2} + \epsilon^3 g_3 + \epsilon^{7/2}g_{7/2} + \cdots, \tag{4.2a}$$

$$h = \epsilon^{5/2}h_{5/2} + \epsilon^3 h_3 + \epsilon^{7/2}h_{7/2} + \cdots, \tag{4.2b}$$

$$\varphi = \epsilon^{5/2}\varphi_{5/2} + \epsilon^3\varphi_3 + \epsilon^{7/2}\varphi_{7/2} + \cdots, \qquad \Psi = \epsilon^{7/2}\Psi_{7/2}, \tag{4.3}$$

where $H_0 \neq -G_0$. (We have freely altered the scaling of Ψ in (4.3) on the grounds that this forcing is added solely as a device to excite the unstable mode.)

We develop the equations once again: at leading order ($\epsilon^{5/2}$), we find the neutral-mode solution,

$$g_{5/2} = -\frac{G_0'}{v}\varphi_{5/2}, \qquad h_{5/2} = -\frac{H_0'}{v}\varphi_{5/2} \qquad \text{and} \qquad \varphi_{5/2} = A(T)e^{ix} + \text{c.c.} \tag{4.4}$$

In this instance, singularities occur at the critical point at leading order because $H_{0*}' \neq 0$. We now recognize these problems as symptoms of a critical region surrounding the critical point; we press on to higher order to discover the critical-region scalings and to complete the outer solution.

At the following order (ϵ^3),

$$g_3 = -\frac{G_0'}{v}\varphi_3 \qquad \text{and} \qquad h_3 = -\frac{H_0'}{v}\varphi_3, \tag{4.5}$$

and at $O(\epsilon^{7/2})$,

$$\left.\begin{aligned} g_{7/2} + \frac{G_0'}{v}\varphi_{7/2} &= -\frac{G_1'}{v}Ae^{ix} - \frac{G_0'}{v^2}iA_T e^{ix} + \text{c.c.}, \\ h_{7/2} + \frac{H_0'}{v}\varphi_{7/2} &= -\frac{H_1'}{v}Ae^{ix} - \frac{H_0'}{v^2}iA_T e^{ix} + \text{c.c.} \end{aligned}\right\} \tag{4.6}$$

It turns out that $g_3 = h_3 = \varphi_3 = 0$; the correct critical-region scaling is therefore once again $v = O(\epsilon)$. As we approach that region, $h \to O(\epsilon^{3/2})$, which partly guides our inner expansion.

4.2. The critical region

Inside the critical region, we set $v = \epsilon Y$ and pose the sequences,

$$\left.\begin{array}{l} g \to Z(x, Y, T) = \epsilon^2 Z_2 + \epsilon^{5/2} Z_{5/2} + \cdots, \\[2mm] h \to W(x, Y, T) = \epsilon^{3/2} W_{3/2} + \epsilon^2 W_2 + \epsilon^{5/2} W_{5/2} + \cdots \end{array}\right\} \qquad (4.7)$$

The fields Z and W satisfy

$$Z_T + Y Z_x + \tfrac{1}{2}\epsilon^{-2}\varphi_x\left[(\kappa - 1)Z_Y + (\kappa + 1)W_Y\right] = -\varphi_x(G'_{1*} + Y G''_{0*} + \cdots) \qquad (4.8)$$

and

$$W_T + Y W_x + \tfrac{1}{2}\epsilon^{-2}\varphi_x\left[(\kappa + 1)Z_Y + (\kappa - 1)W_Y\right] = -\epsilon^{-1}\varphi_x(H'_{0*} + \epsilon H'_{1*} + \epsilon Y H''_{0*} + \cdots). \qquad (4.9)$$

We turn the handle of the crank of perturbation theory: at order $\epsilon^{3/2}$,

$$W_{3/2T} + Y W_{3/2x} = -H'_{0*}(iAe^{ix} + \text{c.c.}), \qquad (4.10)$$

giving,

$$W_{3/2} = -iH'_{0*}\varpi e^{ix} + \text{c.c.}, \qquad \varpi(Y, T) = \int_0^T A(s)e^{iY(s-T)}\, ds, \qquad (4.11)$$

if $W_{3/2}(x, Y, 0) = 0$. Note that $\int_{-\infty}^{\infty} \varpi(Y, T)\, dY = \pi A$ and $\varpi \sim -iY^{-1}A$ for large $|Y|$, or equivalently $W_{3/2} \sim -Y^{-1}H'_{0*}\varphi_{5/2} \equiv -\epsilon v^{-1}H'_{0*}\varphi_{5/2}$.

At $O(\epsilon^2)$, we have

$$Z_{2T} + Y Z_{2x} = -\frac{\kappa + 1}{2}W_{3/2Y}(iAe^{ix} + \text{c.c.}) \qquad (4.12)$$

and

$$W_{2T} + Y W_{2x} = -\left(\frac{\kappa - 1}{2}W_{3/2Y} + H'_{0*}\right)(iAe^{ix} + \text{c.c.}), \qquad (4.13)$$

with the solution,

$$Z_2 = \frac{\kappa + 1}{2}H'_{0*}J \qquad \text{and} \qquad W_2 = \frac{\kappa - 1}{2}H'_{0*}J - H'_{0*}\partial_x\int_0^T \varphi_3(x + Y(s - T), s)\, ds, \qquad (4.14)$$

where

$$J(x, Y, T) = J_0(Y, T) + [J_2(Y, T)e^{2ix} + \text{c.c.}], \qquad (4.15)$$

$$J_0 = \int_0^T [A(s)\varpi^*(Y, s) + A^*(s)\varpi(Y, s)]_Y\, ds, \qquad (4.16a)$$

$$J_2 = -\int_0^T e^{2iY(s-T)}[A(s)\varpi(Y, s)]_Y\, ds. \qquad (4.16b)$$

Note that $\int_{-\infty}^{\infty} J(x, Y, T)\, dY = 0$ and $Z_2 \sim O(Y^{-3}) = O(\epsilon^3 v^{-3})$ for large $|Y|$.

Lastly, at $O(\epsilon^{5/2})$,

$$Z_{5/2T} + Y Z_{5/2x} = -\left(\frac{\kappa - 1}{2}Z_{2Y} + \frac{\kappa + 1}{2}W_{2Y} + G'_{1*} + Y G''_{0*}\right)(iAe^{ix} + \text{c.c.})$$

$$\qquad\qquad - \varphi_{3x}\frac{\kappa + 1}{2}W_{3/2Y}, \qquad (4.17)$$

and

$$W_{5/2T} + Y W_{5/2x} = -\left(\frac{\kappa+1}{2} Z_{2Y} + \frac{\kappa-1}{2} W_{2Y} + H_{1*}' + Y H_{0*}''\right)(iAe^{ix} + \text{c.c.})$$
$$- \varphi_{3x}\frac{\kappa-1}{2} W_{3/2Y} - \varphi_{7/2x} H_{0*}'. \tag{4.18}$$

Only the solution for $Z_{5/2}$ is required in what follows and this is

$$Z_{5/2} = -G_{0*}'' \varphi_{5/2} + \int_0^T e^{iY(s-T)}\left[G_{0*}'' A_s - iA G_{1*}' - \frac{\kappa^2-1}{2}(iAJ_{0Y} - iA^* J_{2Y})\right]ds. \tag{4.19}$$

We also now see that $Z \sim -\epsilon^{5/2} G_{0*}'' \varphi_{5/2}$ and $W \sim -\epsilon^{5/2} v^{-1} H_{0*}' \varphi_{5/2}$ as we move out of the critical region, which matches straightforwardly with the inner limit of the outer solution.

4.3. The amplitude equation

Once again, we construct the integral for φ by defining another uniformly valid solution. This time,

$$\varphi_{xx} - \Psi_{xx} = \epsilon^{5/2}\int_{-\infty}^{\infty} g_{5/2}\, dv + \epsilon^3 \int_{-\infty}^{\infty} g_3\, dv$$
$$+ \epsilon^{7/2}\left[\mathscr{P}\int_{-\infty}^{\infty} g_{7/2}\, dv + \mathscr{P}\int_{-\infty}^{\infty}(Z_{5/2} - Y g_{5/2*})\, dY\right]. \tag{4.20}$$

The $O(\epsilon^{5/2})$ terms reproduce the neutral stability condition. At order ϵ^3, we find that $\varphi_{3xx} + \varphi_3 = 0$. The nontrivial solution describes a redundant correction to the amplitude of the neutral mode, and so we may take $\varphi_3 = 0$, which further implies that $g_3 = h_3 = 0$, as remarked earlier.

At order $\epsilon^{7/2}$, we arrive at the relation,

$$I_0 A_T + iI_1 A + \hat{\Psi}_{7/2} = \langle e^{-ix}(Z_{5/2} - Y g_{5/2*})\rangle, \tag{4.21}$$

after projection onto the fundamental wavenumber, where $\hat{\Psi}_{7/2}$ is the projection of the external forcing. Finally, we introduce the explicit solution for $Z_{5/2}$, leading to the nonlocal amplitude equation,

$$A_T = \frac{i(I_1 + i\pi G_{0*}'')}{(I_0 + i\pi G_{1*}')} A$$
$$- \frac{\pi(1-\kappa^2)H_{0*}'}{(I_0 + i\pi G_{1*}')}\int_0^{T/2}\int_s^{T-s} s^2 A(T-s)A(s')A(s'-s)\, ds'\, ds + \chi(T), \tag{4.22}$$

with $\chi(T)$ again a suitable forcing function. This equation can be scaled into a standard form in order to eliminate some of the distracting constants.

In form, (4.22) is identical to the nondissipative version of the equations derived by Hickernell (1984), Goldstein and Leib (1989) and Berk et al. (1996). The analysis of the equation presented by Goldstein and Leib reveals the unappealing feature that the solution does not saturate. In fact, once nonlinearity comes into play, the growth of the mode accelerates and diverges in finite time. The divergence of the solution is approximately given by

$$A = C(T_s - T)^{-5/2}\exp i[\theta - \sigma\log(T_s - T)] \tag{4.23}$$

(Goldstein and Leib 1989), where T_s is the time of divergence, θ is an arbitrary

phase, and C and σ are real constants that are determined by the relations,

$$C^2 = \frac{\sigma(5 + 2i)(I_0 + i\pi G'_{1*})}{2\pi(1 - \kappa^2)H'_{0*}D(\sigma)}, \qquad D(\sigma) = \int_1^\infty \int_v^\infty \frac{(v - 1)^2 \, du \, dv}{[uv(u + v - 1)]^{i\sigma + 5/2}}. \qquad (4.24)$$

The amplitude equation cannot therefore capture the saturation of the instability, and merely describes a transient in the evolution. The divergence of $A(T)$ predicted by (4.22) is, of course, unphysical, and simply reflects the passage of the mode amplitude out of the asymptotic regime. For this reason, we do not solve the amplitude equation in detail, and instead refer the reader to the previous articles. The failure of the amplitude equation to predict the saturation level is disappointing, and we turn to numerical computations to resolve the issue in the next section. Interestingly, the singular solution is constructed by dropping the linear term in (4.22), and thus exists even if the equilibrium is stable, implying the existence of finite-amplitude, subcritical instability (see also Berk et al. 1999).

5. Numerical computations

We complement the asymptotic theory with a series of numerical computations. We solve the two-species equations (2.1) and (2.2) using another operator-splitting algorithm (Cheng and Knorr 1976). We select the computational domain, $0 \leqslant x \leqslant 2\pi$ and $-4 \leqslant v \leqslant 4$, and an initial condition given by an equilibrium profile of the form (2.3). The disturbance is introduced by forcing the electric field potential with a term, $F_0 t e^{-10t^2} \cos x$, where F_0 is a small constant (typically taken to be 10^{-3}). We used various resolutions depending on the computations performed. The shorter runs used to estimate the amplitude at which nonlinearity became important had 64 grid points in x (32 Fourier modes) and up to 2000 gridpoints in v. The longer runs that explored the saturation process typically had approximately 512 and 2000 gridpoints in x and v, respectively. Overall, we attempted to minimize integration and resolution errors wherever possible by taking sufficiently small timesteps and fine grids. However, a key feature of the dynamics is a continual production of increasingly fine spatial scales, which eventually results in resolution error. Thus, whilst we have confidence in the shorter-time computations, the results at long times are less reliable. At those late times, the computations are underresolved and an artificial dissipation operates (Cheng and Knorr 1976) that is difficult to quantify and control. This is especially unsatisfying because the ultimate fate of the system is not revealed until such times, and we had no choice but to use the less reliable runs to explore the late stages with resolutions of (128×2000) gridpoints.

5.1. Scaling data

The disturbance introduced in the potential excites the unstable normal mode which grows exponentially until nonlinear effects come into play. To measure the amplitude of the disturbance, we use the quantity

$$\Phi(t) = \left[\frac{1}{4\pi} \int_0^{2\pi} \varphi^2 \, dx \right]^{1/2} = \left[\sum_{n=1}^\infty |\hat{\varphi}_n(t)|^2 \right]^{1/2}, \qquad (5.1)$$

where $\hat{\varphi}_n(t)$ denote the Fourier mode amplitudes of φ. When the spectrum is dominated by the longest, single wave, $\Phi \approx |\varphi_1| \equiv |A|$. Typical time series of $\Phi(t)$ are shown in Fig. 7, and illustrate the termination of exponential growth and the onset
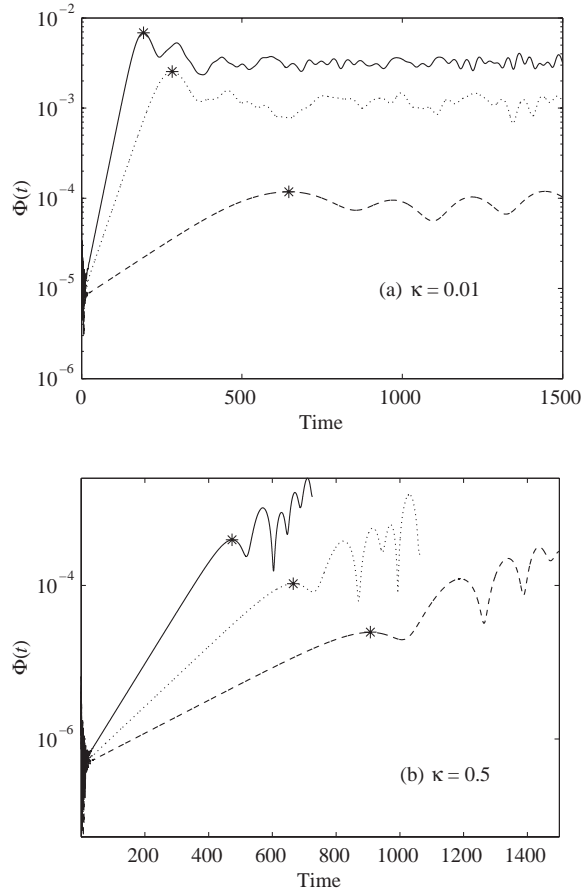
Figure 7. Sample time series of the amplitude measure, $\Phi(t)$, for $k = 1$. In (a), $\kappa = 0.01$ with $a = 0.19$ (dashed), 0.22 (dotted) and 0.25 (solid). In (b), $\kappa = 0.5$ with $a = 0.22$ (dashed), 0.2275 (dotted) and 0.24 (solid). The stars indicate the measurements of Φ_m.

of trapping oscillations. The oscillations reflect nonlinear effects and so we estimate the amplitude threshold for which nonlinearity becomes important by measuring the level of the first peak in the time series, Φ_m (see Fig. 7). For $\kappa = 0.5$, saturation does not occur beyond the first maximum, unlike at $\kappa = 0.01$.

In Fig. 8 we plot Φ_m against both the distance to the stability boundary, $a - a_0$, and the growth rate of linear theory, $\eta \equiv c_i$. The peak amplitude scales with either $a - a_0$ or η in accordance with the predictions of the asymptotic theory: $\Phi_m \sim (a - a_0)^2$ for $\kappa \sim (a - a_0)$ or smaller, and $\Phi_m \sim (a - a_0)^{5/2}$ for $\kappa \gg (a - a_0)$. Note the distinctive crossover in scaling when $(a - a_0)$ is slightly less than κ.

Also included in Fig. 8 is the corresponding data for the single-species case, $\kappa = 0$. This case permits a simple comparison with the single-wave model, and is obtained as follows. From the single-wave model with the appropriate value of β (which is approximately 0.4 for $k = 1$), we compute the amplitude of the first maximum in $|A(T)|$ (cf. Fig. 5). With the scalings of Sec. 3.4, we then reconstruct the original Φ_m. An analogous comparison for $0 < \kappa \ll 1$ entails time-consuming computations with many different values for μ which we have not performed. Instead, we opt for detailed comparisons of a few computations, as given below.
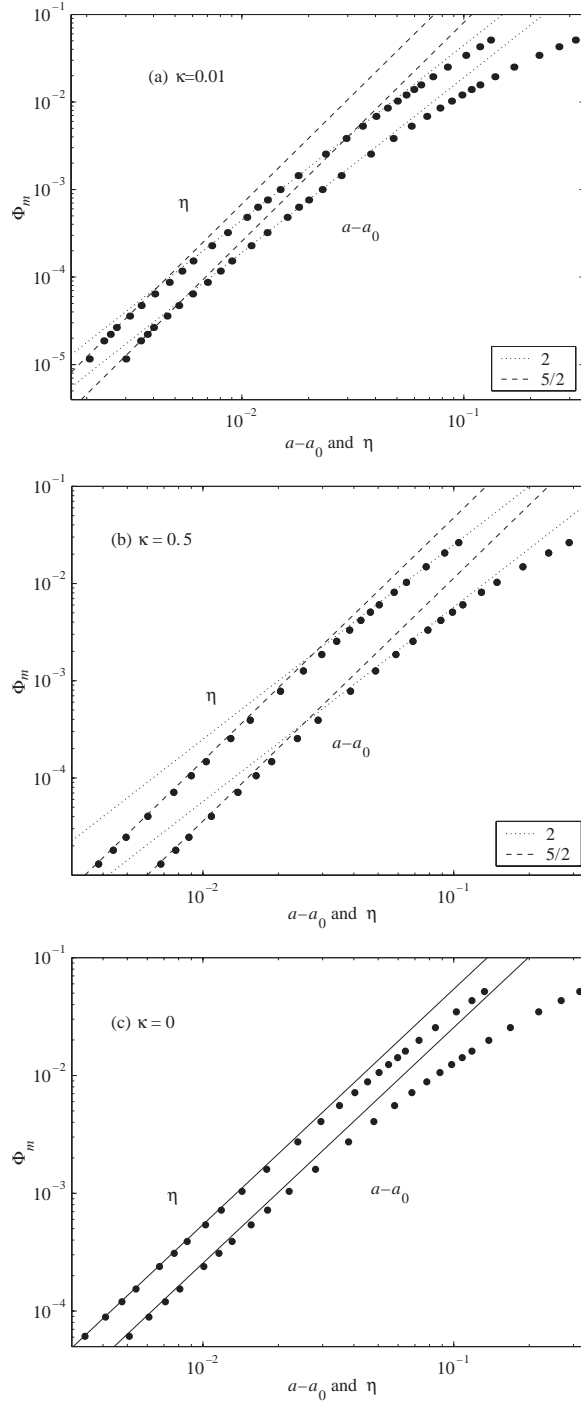
Figure 8. Scaling data for $\kappa = 0.01$ and 0.5. $k = 1$. Plotted is the amplitude of the first peak in $\Phi(t)$ (the quantity defined in (5.1)), denoted by Φ_m, versus either the distance to the stability boundary, $a - a_0$, or the linear growth rate, $\eta = kc_i$. The trends of the trapping and singular scalings are shown by dotted and dashed lines, respectively. In panel (c), we show the corresponding result for $\kappa = 0$, together with the scalings predicted by the single-wave model (solid lines).
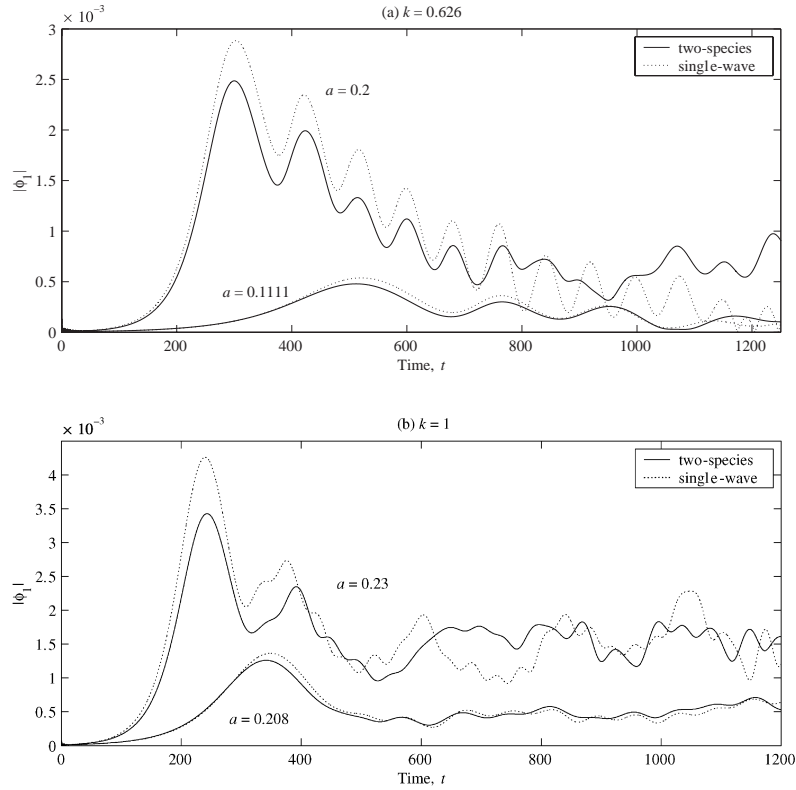
Figure 9. Time series of $\Phi(t)$ for (a) $k = 0.626$, $a = 0.1111$ and $a = 0.12$, and (b) $k = 1$, $a = 0.208$ and $a = 0.23$ ($\kappa = 0.01$). In each case, the results are compared with the predictions of the modified single-wave model. In (a) $\beta = 0$ and $\mu = 0.5$ and 0.25, and in (b) $\beta = 0.4$ and $\mu = 0.25$ and 0.15. The corresponding normal-mode eigenvalues in (a) are $c_{\text{num}} = 1.777 + 0.0107i$ and $1.762 + 0.0242i$ (computed numerically from the dispersion relation), in comparison to $c_{\text{swm}} = 1.777 + 0.0112i$ and $1.761 + 0.0261i$ (calculated by reconstruction from (3.26)). In (b), $c_{\text{num}} = 1.523 + 0.0167i$ and $1.501 + 0.0307i$, in comparison to $c_{\text{swm}} = 1.516 + 0.0178i$ and $1.509 + 0.0278i$.

5.2. *Heavy ions*

Some further details of solutions with $\kappa \ll 1$ are shown in Figs 9 and 10. The first figure compares $\Phi(t)$ with the corresponding result reconstructed from the mode amplitude $|A(t)|$ of the modified single-wave model; the time series agree qualitatively, at least for shorter times. Also compared in the caption are the corresponding normal-mode eigenvalues computed numerically from the dispersion relation and analytically from the single-wave model. The main source of disagreement arises because we cannot take $a - a_0$ to be too small (which is where the weakly nonlinear theory is most accurate) whilst remaining within the single-wave regime for $\kappa = 0.01$.

Snapshots of the electron distribution function for $\kappa = 0.01$, $a = 0.24$ and $k = 1$ are shown in Fig. 10. The magnification of the critical region illustrates how the distribution twists up into a localized cat's eye structure, which drifts to larger v over longer times, exactly as predicted by the single-wave model. By the time of the final snapshots, however, the cat's eye has drifted out of the regime of that model.

Although the results are less reliable, we continue the computations to longer
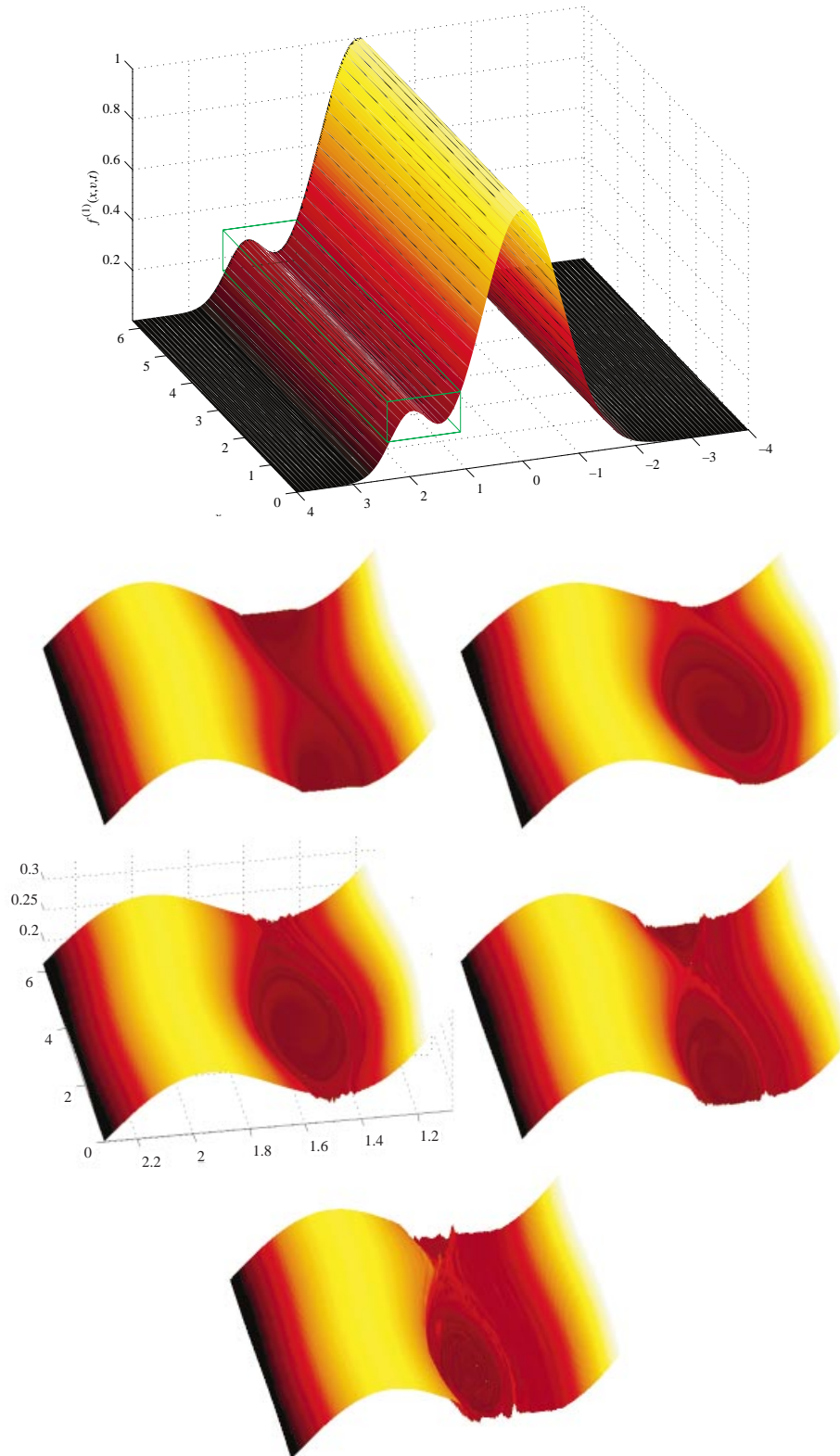
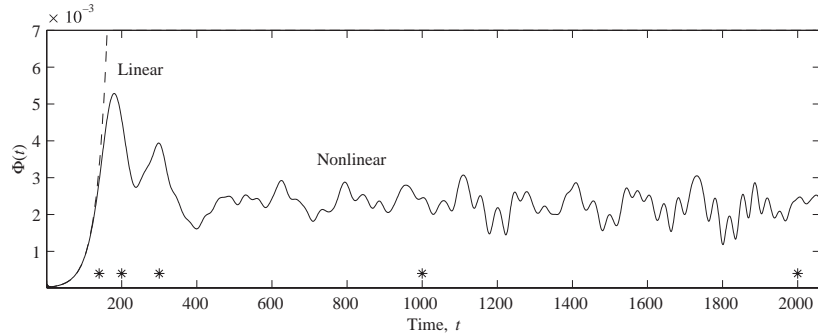**Figure 10.** For caption see facing page.

Figure 10 (cont.). The top panel (on facing page) shows an initial electron distribution for $a = 0.24$, $k = 1$ and $\kappa = 0.01$, plotted as a surface above the (x, v)-plane. Displayed next are five snapshots of magnifications of the distribution in the vicinity of the critical region at $t = 140, 200, 300, 1000$ and 2000. The evolution of the mode amplitude $\Phi(t)$ is shown above (the stars indicate the times of the preceding snapshots).

times in order to uncover what happens when the cat's eye reaches the peak of the destabilizing bump. As shown in Fig. 11, the drift peters out and the trapping oscillations in $\Phi(t)$ become more irregular, occasionally bursting to higher amplitude. The bursts appear to be connected with the formation of secondary vortical structures in the wake of the main cat's eye (see the first panel of Fig. 11), and persist whilst the main vortex interacts strongly with the peak. Ultimately, however, the mode enters a protracted final decline that we attribute to the continued Landau damping by the positive ions, which remain largely undisturbed throughout (see the final snapshot of the positive-ion distribution in Fig. 11). By this time, the electron distribution is significantly rearranged, although a nonmonotonic remnant of the bump still survives.

5.3. Comparable ion masses

Now we turn to the singular case. In Figs 12 and 13 we show results from a computation with $k = 1$, $a = 0.25$ and $\kappa = 0.5$. As anticipated from the diverging, nonlocal amplitude equation, the mode amplitude reaches a first maximum that is merely a temporary interruption of the linear growth and is much smaller than the maxima reached somewhat later. The mode amplitude eventually settles into a train of erratic oscillations. Early in the computation, the amplifying disturbance again begins to twist up the distribution inside a localized region contained within the unstable gradients of the electron distribution function. Unlike in the single-wave case, however, the thickness of this region continues to grow, and the nucleated structures drift rapidly in velocity. Notably, a vortex-like hole in the electron distribution passes through the bump near $t = 1000$ (Fig. 12), and the x-averaged distribution becomes significantly flattened at later times. Simultaneously, there is some crenellation of the positive-ion distribution (Fig. 13), though the effect is far less spectacular.

A suite of longer-time computations are shown in Fig. 14. Despite the different parameter values in each of the computations, the final states of the computations are all quite similar, consisting of a significantly flattened x-averaged electron distribution with an erratically varying mode amplitude. Figure 14 reveals the rather surprising result that characteristic measures of $\Phi(t)$ do not scale in a clear way with the distance to the stability boundary. For example, both the maximum amplitude
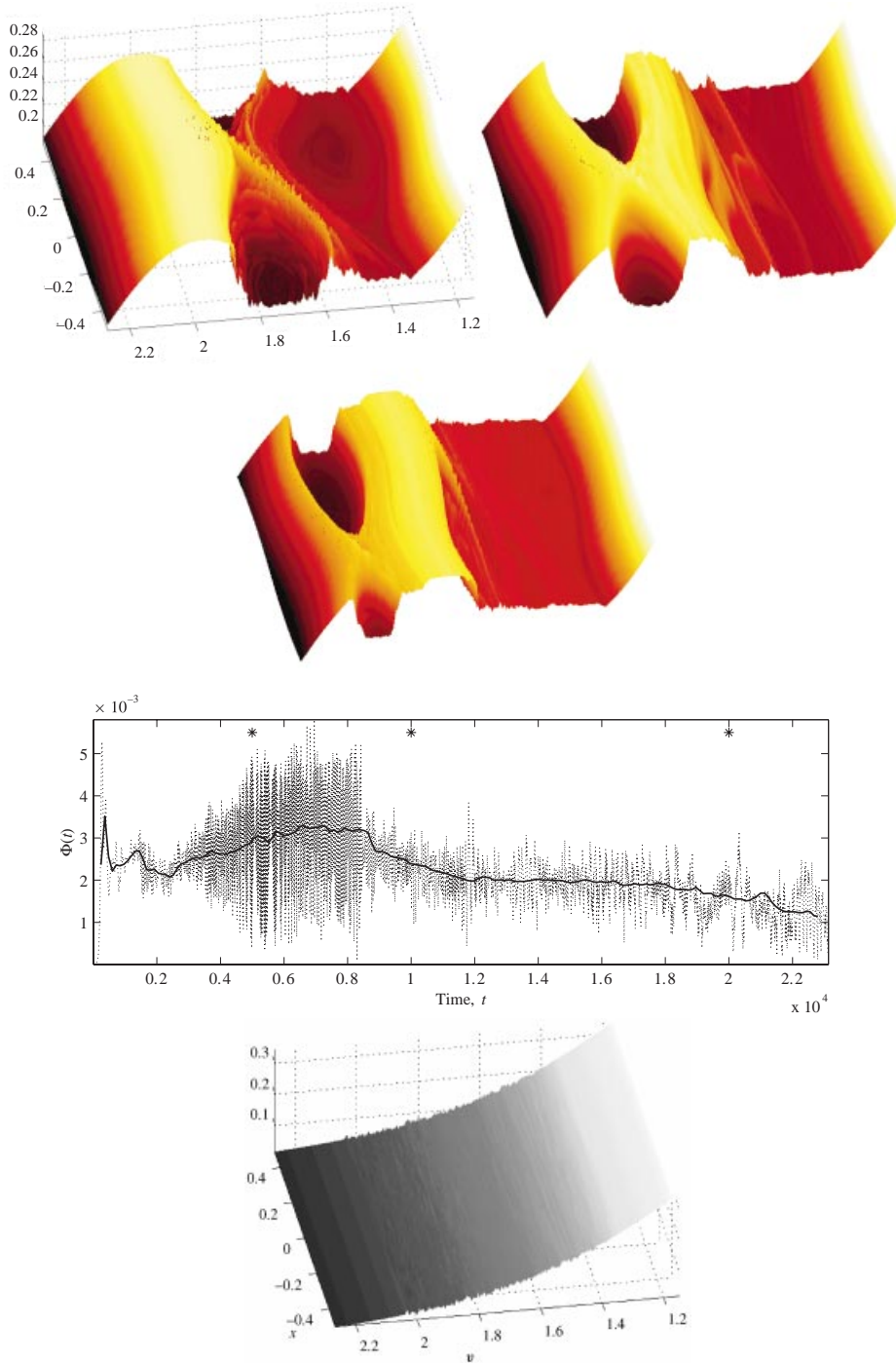
Figure 11. Magnifications of the electron distribution in the vicinity of the critical region at $t = 5000$, $10\,000$ and $20\,000$, for the continuation of the computation shown in Fig. 10. The evolution of the mode amplitude $\Phi(t)$ is shown below (by a dotted line; the stars indicate the times of the snapshots and the solid line shows a running average over 1000 time units) together with the magnification of the positive-ion distribution at $t = 20\,000$. $a = 0.24$, $k = 1$ and $\kappa = 0.01$.
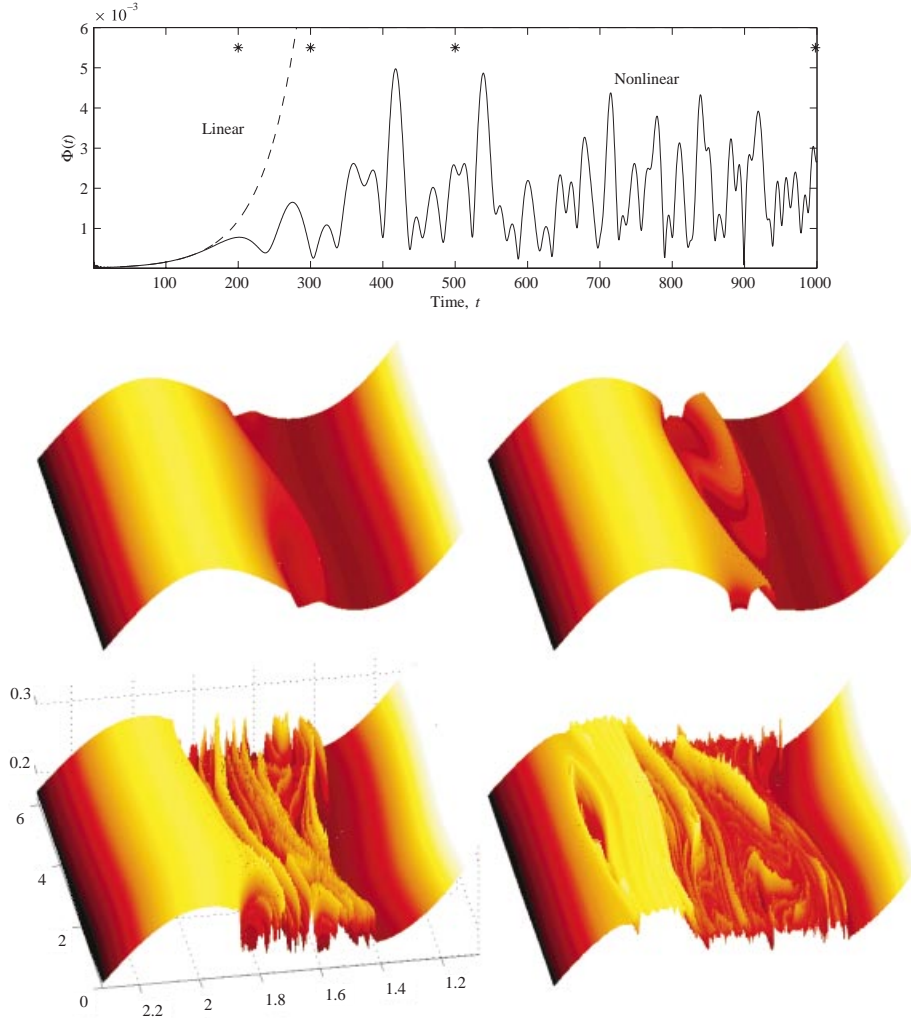
Figure 12. A computation with $a = 0.25$, $k = 1$ and $\kappa = 0.5$. The evolution of the mode amplitude, $\Phi(t)$, is shown in the top panel. Below are displayed four snapshots of the electron distribution in the vicinity of the critical region at $t = 200$, 300, 500 and 1000.

reached during the computations and the typical mean level at later times are comparable in all the cases, and, in fact, depend nonmonotonically on $a - a_0$ (the computations with intermediate values for $a - a_0$ have the lowest final mean level, and at $k = 0.728\,425$, the computation nearest the stability boundary reaches the largest maximum amplitude). Therefore, even though the singular scaling correctly predicts the onset of nonlinearity, we are unable to provide a scaling law that predicts the typical amplitude level beyond that onset, at least using the electric field.

Evolution over an even longer timescale is shown in Fig. 15 for $a = 0.25$. This illustrates a further surprising result that the mode amplitude does not eventually decline, but looks to converge to a finite value. Therefore, the damping effect of the positive ions must somehow be arrested at larger κ. A glance at the final snapshot of the distribution functions reveals why the Landau damping becomes ineffective: the
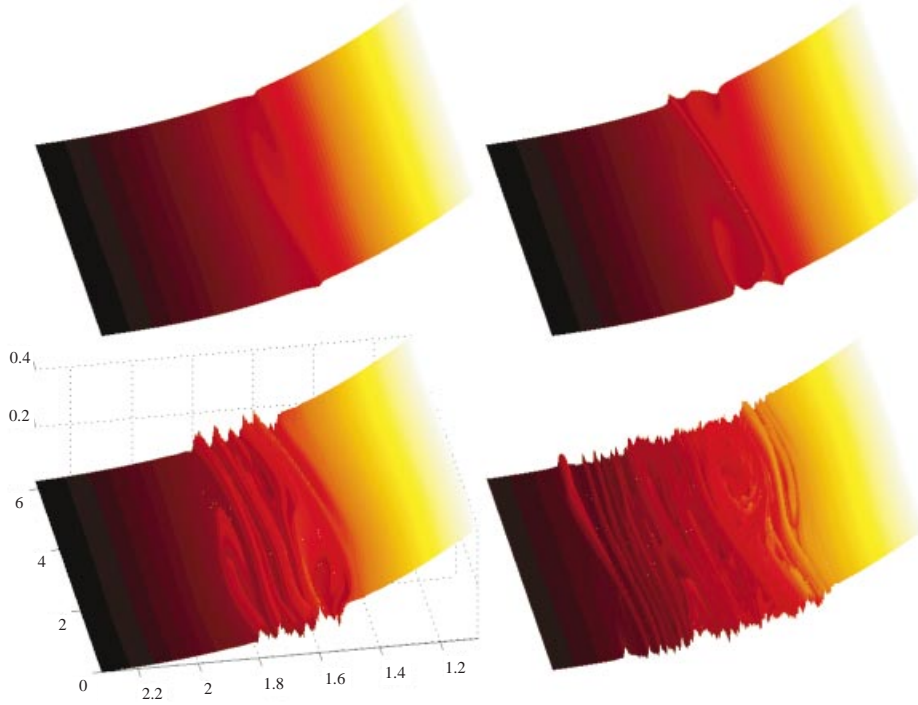
Figure 13. Four snapshots of the positive-ion distribution in the vicinity of the critical region at $t = 200, 300, 500$ and 1000 for the computation shown in Fig. 12.

positive-ion distribution twists up into independent cat's eyes (unrelated secondary structures are visible in both distributions). The winding action of the cores of these structures removes the gradients that Landau damps the negative ions, and leaves a staircase structure in the x-average. Moreover, the structures appear where the negative-ion distribution has already been flattened, negating any effect the electrons might otherwise have.

6. Discussion

In this article we have considered the nonlinear dynamics of two-species electrostatic instabilities. The central issue is how the saturation level of the instability, as measured in the electric field, A_{sat}, varies with the distance to the stability boundary, ϵ (or, equivalently, the growth rate). Previous studies had presented conflicting answers to this problem, predicting three different scaling laws: $A_{\text{sat}} \sim \epsilon^{\alpha}$, with $\alpha = \frac{1}{2}$ (Hopf), 2 (trapping) or $\frac{5}{2}$ ('singular', as we have termed it), and a dependence on $\kappa = |(e_2 m_1)/(e_1 m_2)|$, a dimensionless combination of the two charge-mass ratios. Our results shed further light on the correct saturation level for ideal plasmas with periodic spatial boundaries, subject to a classical bump-on-tail instability. Specifically, *none of the scalings accurately predict the saturation amplitude.* By way of conclusion, we summarize our findings in detail.

When $\kappa = 0$, the correct scaling law is trapping (as already indicated by Crawford (1995) and del Castillo-Negrete (1998)). At a level predicted by this scaling, the instability saturates and trapping oscillations occur in the mode amplitude. The
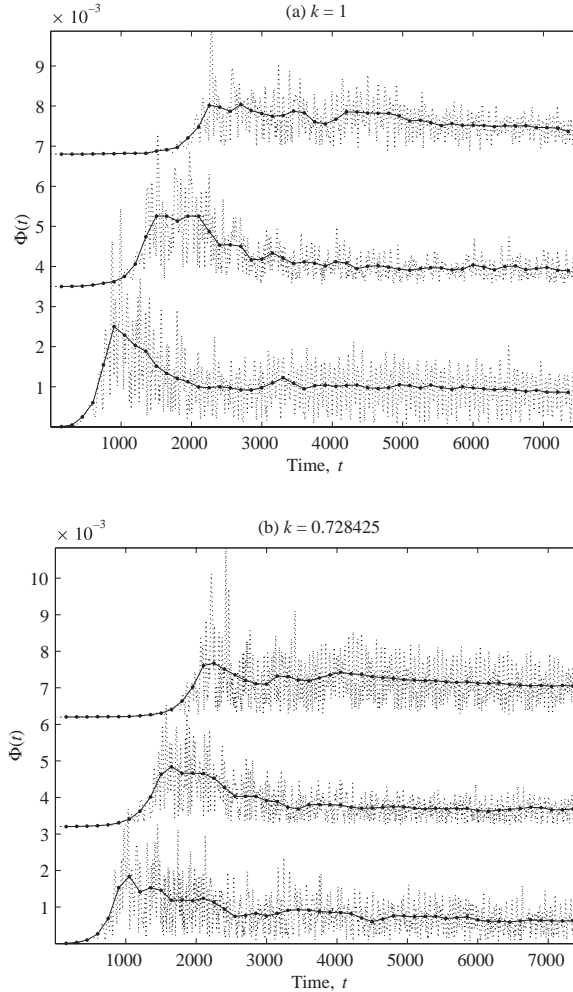
Figure 14. The mode amplitudes, $\Phi(t)$, for a sequence of runs with different a and two values for k: (a) $k = 1$ and (b) $k = 0.728\,425$ (the second k-value characterizes equilibrium profiles that limit to the minimum of the stability boundary for $\kappa = 0.5$). In (a), the runs have $a = 0.217$, 0.222 and 0.231. In (b), $a = 0.18$, 0.185 and 0.195. The dotted line shows the actual amplitude, and the solid line and dots show a running average (over 150 time units). In each case, the curves are offset for the sake of clarity; the value of a decreases as one moves up the curves (the weakening of the linear instability is seen as the increasingly delayed emergence of the mode).

main effect on the distribution function is localized within a narrow velocity range surrounding the pattern speed of the unstable mode (the critical region) that is far narrower than the scale of the bump.

If κ is small (order ϵ or smaller), nonlinearity again becomes important at the trapping scaling, and the main effect of instability is once again confined to a narrow critical region. Thereafter, the mode amplitude subsides due to Landau damping by positive ions, but then enters a quasi-steady regime in which the critical region slowly expands as vortex-like structures embedded in the distribution function drift in velocity. Ultimately, the affected region spans a far larger velocity spread than
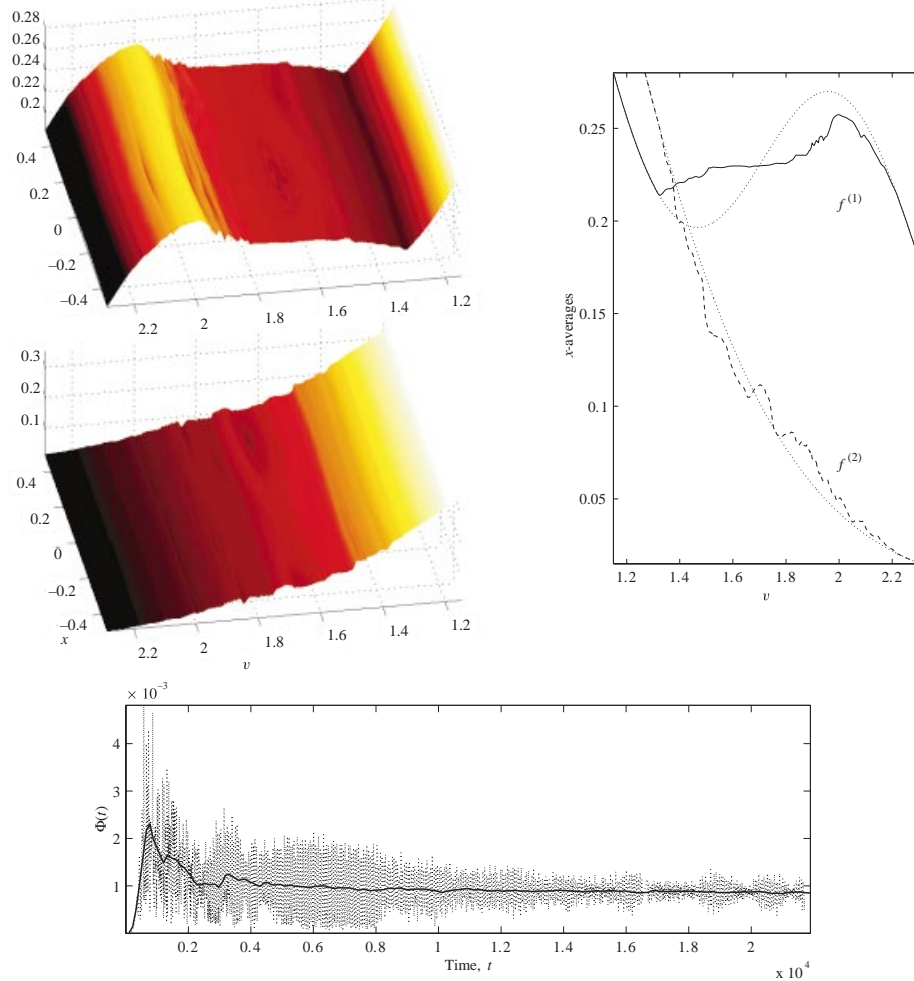
Figure 15. Magnifications in the vicinity of the critical regions of the electron and positive ion distributions at $t = 20\,000$ for $\kappa = 0.5$ and $a = 0.25$ (the continuation of the computation shown in Fig. 12). The x-averages are also shown, together with the equilibrium profiles. The lowest panel shows the time series of $\Phi(t)$ (dotted line), including a running average (over 200 time units; solid line).

expected from the trapping scaling, and the destabilizing bump is substantially eroded. At that stage, bursting, erratic trapping oscillations occur, but eventually the mode amplitude enters a final decline.

For larger values of κ, nonlinearity first comes into play with the singular scaling $\alpha = \frac{5}{2}$, but this is not the saturation level, and the mode continues to grow. The disturbance still remains confined to a critical region. However, that region evolves rapidly and spreads quickly, halting when the disturbance spans a region enveloping the destabilizing bump. The typical electric field amplitude at this stage has an unobvious dependence on ϵ, and we find no clear scaling law for the level of saturation. Unlike the dynamics at small κ, the mode may survive for long times due to the rearrangement of the positive-ion distribution and the creation of secondary vortical structures in that distribution.

Overall, we are unable to characterize the dynamics by a single-amplitude scaling based on the electric field: depending on the size of κ, the system passes through several stages, each with its own characteristic measure of mode amplitude. A better estimate for the strength of the instability is based not on the electric field, but on the conclusion that the mode eventually suppresses much of the nonmonotonic profile of the x-averaged electron distribution, $f^{(1)}$, over the bump region. For example, consider the change to the particle kinetic energy as $t \to \infty$:

$$\langle v^2(f^{(1)} - F^{(1)}) \rangle \equiv \int_0^{2\pi} \int_{-\infty}^{\infty} v^2 [f^{(1)}(x,v,t) - F^{(1)}(v)]\, dv \frac{dx}{2\pi} \sim \begin{cases} \epsilon & \text{Hopf} \\ \epsilon^3 & \text{trapping} \\ \epsilon^{7/2} & \text{singular} \\ \varepsilon^{3/2} & \text{actual,} \end{cases} \quad (6.1)$$

where ϵ is the customary distance to the stability boundary, but ε measures the peak-to-trough size of the bump, which in turn implies that the velocity spread of the bump region is $O(\varepsilon^{1/2})$. (Only for $\kappa = 0$ and at the minimum of the stability boundary is it true that $\epsilon = \varepsilon$.) The estimate for the Hopf scaling is based on a nonlinear perturbation of amplitude $\epsilon^{1/2}$ covering an order of unity velocity spread (the usual dissipative estimate, with no critical-layer structure, for which the instability affects the mean at order ϵ). The trapping and singular scaling estimates follow because the critical region has width ϵ and disturbance amplitude ϵ^2 or $\epsilon^{5/2}$. Neither of these correctly estimate the strength of the instability because the distribution is significantly rearranged over the region of the bump, leading to a quite different result, $\varepsilon^{3/2}$.

A crucial ingredient is therefore that the strength of the mode is measured by the shape of the initial electron profile, rather than the distance to the stability boundary. This premise is somewhat similar to Gardner's ideas concerning the energy available to the electric field through rearrangements of the electron distribution, which follow from a consideration of the energy conservation law (Gardner 1963). For our particular form of the the two-species problem, energy conservation can be written as

$$\frac{1}{2}\langle v^2 f^{(1)} \rangle + \frac{1}{2\kappa}\langle v^2 f^{(2)} \rangle + \frac{1}{2}\int_0^{2\pi/L} \varphi_x^2 \frac{dx}{2\pi} = \text{constant}, \quad (6.2)$$

once the forcing potential has been turned off. Gardner's argument proceeds by observing that, since $f^{(1)}$ can only be rearranged by the dynamics, there is a minimum possible kinetic energy contained in the electrons, $\langle v^2 f_R \rangle / 2$. The function $f_R(v)$ is obtained from a suitable rearrangement of the initial electron distribution, $F^{(1)}(v)$, which preserves the area of phase space and makes that distribution monotonic in $v > 0$. Thus, provided the initial perturbations about the equilibrium state introduced by the external forcing are small,

$$\frac{1}{2\kappa}\langle v^2(f^{(2)} - F^{(2)}) \rangle + \frac{1}{2}\int_0^{2\pi/L} \varphi_x^2 \frac{dx}{2\pi} \approx \frac{1}{2}\langle v^2(F^{(1)} - f^{(1)}) \rangle \leqslant \frac{1}{2}\langle v^2(F^{(1)} - f_R) \rangle. \quad (6.3)$$

Moreover, since $F^{(2)}$ is already monotonic for $v > 0$, any rearrangement of the positive ions can only add to the kinetic energy contained in that species. Hence,

$$\frac{1}{2}\int_0^{2\pi/L} \varphi_x^2 \frac{dx}{2\pi} \leqslant \frac{1}{2}\langle v^2(F^{(1)} - f_R) \rangle. \quad (6.4)$$

We may regard the right-hand side of this inequality as the total free energy available to the system from the electrons. As the instability develops, this energy is tapped and becomes divided between the electric field energy and the kinetic energy of the positive ions. Our estimate for the saturation level is also bounded by this free energy, but is clearly of the same order.

Of course, the time required to reach the state characterized by the alternative scaling does depend strongly upon ϵ, because this parameter controls both the linear growth phase, the onset of nonlinear effects and the drift and expansion of the critical region. The new scaling further implies nontrivial subthreshold dynamics, since bumps can still exist in linearly stable electron distributions when k is suitably chosen. Such dynamics is also evident from the singular solution to Hickernell's amplitude equation (which exists regardless of the sign of the linear growth rate). Indeed, using a suite of numerical computations, we verified that the two-species system is unstable to finite-amplitude perturbations even in the stable regime.

Subthreshold phenomena in two-species plasma has previously been observed by Berman et al. (1985, 1986). Morrison (1987) suggested that this could be the signature of the nonlinear instability of a linearly stable Hamiltonian system. However, we observe a subcritical transition that requires a threshold initial amplitude (see also Berk et al. 1999). We conjecture that nonlinear instability, if it occurs, requires a quite different initial excitation of the system, notably one that changes the x-averaged distribution function (and therefore the reference equilibrium state).

Acknowledgement

References

Balmforth, N. J., Llewellyn Smith, S. G. and Young, W. R. 2000 Disturbing vortices. *J. Fluid Mech.* **426**, 95–133.

Berk, H. L., Breizmann, B. N. and Pekker, M. 1996 Nonlinear dynamics of a driven mode near marginal stability. *Phys. Rev. Lett.* **76**, 1256–1259.

Berk, H. L., Breizmann, B. N., Candy, J., Pekker, M. and Petviashvili, N. V. 1999 Spontaneous hole–clump pair creation. *Phys. Plasmas* **6**, 3102–3113.

Berman, R. H., Tetreault, D. J. and Dupree, T. H. 1985 Simulation of phase space hole growth and the development of plasma turbulence. *Phys. Fluids* **28**, 155–176.

Berman, R. H., Dupree, T. H. and Tetreault, D. J. 1986 Growth of nonlinear intermittent fluctuations in linearly stable and unstable simulation plasma. *Phys. Fluids* **29**, 2860–2870.

Bernstein, I. B., Greene, J. M. and Kruskal, M. D. 1958 Exact nonlinear plasma oscillations. *Phys. Rev.* **108**, 546–550.

Cheng, C. Z. and Knorr, G. 1976 The integration of the Vlasov equation in configuration space. *J. Comp. Phys.* **22**, 330–351.

Churilov, S. M. 1999 Nonlinear stability of a stratified shear flow in the regime with an unsteady critical layer. Part 2. Arbitrary stratification of asymmetric flow. *J. Fluid Mech.* **392**, 233–275.

Churilov, S. M. and Shukhman, I. G. 1987 The nonlinear development of disturbances in a zonal shear flow. *Geophys. Astrophys. Fluid Dyn.* **38**, 145–175.

Crawford, J. D. 1995 Amplitude equations for electrostatic waves: universal behaviour in the limit of weak instability. *Phys. Plasmas* **2**, 97–128.

Crawford, J. D. and Jayaraman, A. 1996 Nonlinear saturation of an electrostatic wave: mobile ions modify trapping scaling. *Phys. Rev. Lett* **77**, 3549–3552.

Crawford, J. D. and Jayaraman, A. 1999 First principles justification of a 'single wave model' for electrostatic instabilities. *Phys. Fluids* **6**, 666–673.

del Castillo-Negrete, D. 1998 Nonlinear evolution of perturbations in marginally stable plasmas. *Phys. Lett.* **241**, 99–104.

Denavit, J. 1981 Simulations of the single-mode, bump-on-tail instability. *Phys. Fluids* **28**, 2773–2777.

Frieman, E., Bodner, S. and Rutherford, P. 1963 Some new results on the quasi-linear theory of plasma instabilities. *Phys. Fluids* **6**, 1298–1305.

Gardner, C. S. 1963 Bound on the energy available from a plasma. *Phys. Fluids* **6**, 839–840.

Goldstein, M. E. and Leib, S. J. 1989 Nonlinear evolution of oblique waves on compressible shear layers. *J. Fluid Mech.* **207**, 73–96.

Hickernell, F. J. 1984 Time-dependent critical layers in shear flows on the beta-plane. *J. Fluid Mech.* **142**, 431–449.

Morrison, P. J. 1987 Variational principle and stability of nonmonotonic Vlasov–Poisson equilibria. *Z. Naturforsch* **42a**, 1115–1123.

O'Neil, T. M., Winfrey, J. H. and Malmberg, J. H. 1971 Nonlinear interaction of a small cold beam and a plasma. *Phys. Fluids* **14**, 1204–1212.

Onishchenko, I. N., Linetskii, A. R., Matsiborko, N. G., Shapiro, V. D. and Shevchenko, V. I. 1971 On nonlinear theory of instability of a monoenergetic electron beam. *Sov. Phys. JETP.* **11**, 281–285.

Simon, A. and Rosenbluth, M. 1976 Single-mode saturation of bump-on-tail instability – immobile ions. *Phys. Fluids* **19**, 1567–1580.